Geol. Mag. **151** (*6*), *2014, pp. 1095–1114. © Cambridge University Press 2014*
doi:10.1017/S0016756814000041

Zircon geochronology of intrusive rocks from Cap de Creus, Eastern Pyrenees

ELENA DRUGUET*†, ANTONIO CASTRO‡, MARTIM CHICHORRO§, M. FRANCISCO PEREIRA¶ & CARLOS FERNÁNDEZ‖

*Departament de Geologia, Universitat Autònoma de Barcelona, 08193 Bellaterra, Barcelona, Spain
‡UA Petrología Experimental, CSIC-Universidad de Huelva, Facultad de Ciencias Experimentales, Campus de El Carmen, 21071 Huelva, Spain
§GEOBIOTEC, FCT, Universidade Nova de Lisboa, Quinta da Torre, 2829-516 Caparica, Portugal
¶Departamento Geociências, ECT, Universidade de Évora, IDL Apt.94, 7001-554 Évora, Portugal
‖Departamento de Geodinámica y Paleontología, Facultad de Ciencias Experimentales, Universidad de Huelva, Campus de El Carmen, 21071 Huelva, Spain

(*Received* 6 November 2013; *accepted* 20 January 2014; *first published online* 11 March 2014)

Abstract – New petrological and U–Pb zircon geochronological information has been obtained from intrusive plutonic rocks and migmatites from the Cap de Creus massif (Eastern Pyrenees) in order to constrain the timing of the thermal and tectonic evolution of this northeasternmost segment of Iberia during late Palaeozoic time. Zircons from a deformed syntectonic quartz diorite from the northern Cap de Creus Tudela migmatitic complex yield a mean age of 298.8 ± 3.8 Ma. A syntectonic granodiorite from the Roses pluton in the southern area of lowest metamorphic grade of the massif has been dated at 290.8 ± 2.9 Ma. All the analysed zircons from two samples of migmatitic rocks yield inherited ages from the Precambrian metasedimentary protolith (with two main age clusters at *c*. 730–542 Ma and *c*. 2.9–2.2 Ga). However, field structural relationships indicate that migmatization occurred synchronously with the emplacement of the quartz dioritic magmas at *c*. 299 Ma. Thus, the results of this study suggest that subduction-related calc-alkaline magmatic activity in the Cap de Creus was coeval and coupled with D_2 dextral transpression involving NNW–SSE crustal shortening during Late Carboniferous – Early Permian time (*c*. 299–291 Ma). Since these age determinations are within the range of those obtained for undeformed (or slightly deformed) calc-alkaline igneous rocks from NE Iberia, it follows that the Cap de Creus massif would represent a zone of intense localization of D_2 transpression and subsequent D_3 ductile wrenching that extended into the Lower Permian during a transitional stage between the Variscan and Cimmerian cycles.

Keywords: granitoid emplacement, late Variscan transpression, migmatite, SHRIMP ages.

1. Introduction

The Cap de Creus massif in the Pyrenees constitutes one of the world's best exposures of rocks displaying ductile deformation structures (Carreras & Druguet, 2013). The area has been intensively studied and mapped by Carreras and Druguet and is a world-class example of shear zones affecting a crystalline basement, and also represents a case-study of metamorphic and magmatic activity contemporaneous with transpressional deformation (Druguet & Hutton, 1998; Druguet, 2001). Field relationships and tectonic analyses clearly suggest that crustal-scale transpression was coeval with magmatic intrusions of varied compositions, and with low-pressure – high-temperature (LP–HT) metamorphism and local partial melting of metasediments. However, neither the petrogenesis of these magmatic rocks, nor the ages of intrusions and associated deformation events have been determined in detail using geochronological data. Our new data may help to constrain the magmatic and tectonic relationships together with the overall tectonic significance of the massif.

†Author for correspondence: elena.druguet@uab.cat

In a regional context, the Cap de Creus massif is considered to be a part of the Variscan basement of NE Iberia (Ábalos *et al.* 2002) and is the easternmost outcrop of the so-called Axial Zone of the Pyrenees (Fig. 1a). Adjacent to the Axial Zone, the Variscan basement also crops out in the North Pyrenean massifs and southwards from the Axial Zone along the Catalan Coastal Ranges. Based on Variscan lithostratigraphic, metamorphic and tectonic features, a zonation has been defined from internal deep-seated rocks, corresponding to the eastern Pyrenean Axial Zone and the North Pyrenean massifs, to more external shallow-seated rocks, corresponding to the western Pyrenean Axial Zone and the southern Catalan Coastal Ranges (Carreras & Capellà, 1994; Druguet, 2001).

Granitoid plutons extensively intrude along and across all these areas (Fig. 1a). However, differences, which are roughly consistent with the abovementioned Variscan zonation, are found among the various granitoid massifs. Thus, most plutons from the Western and Central Pyrenees and from the Catalan Coastal Ranges correspond to epizonal intrusions, characterized by the development of contact metamorphic aureoles and by the lack of ductile solid-state deformations. They have

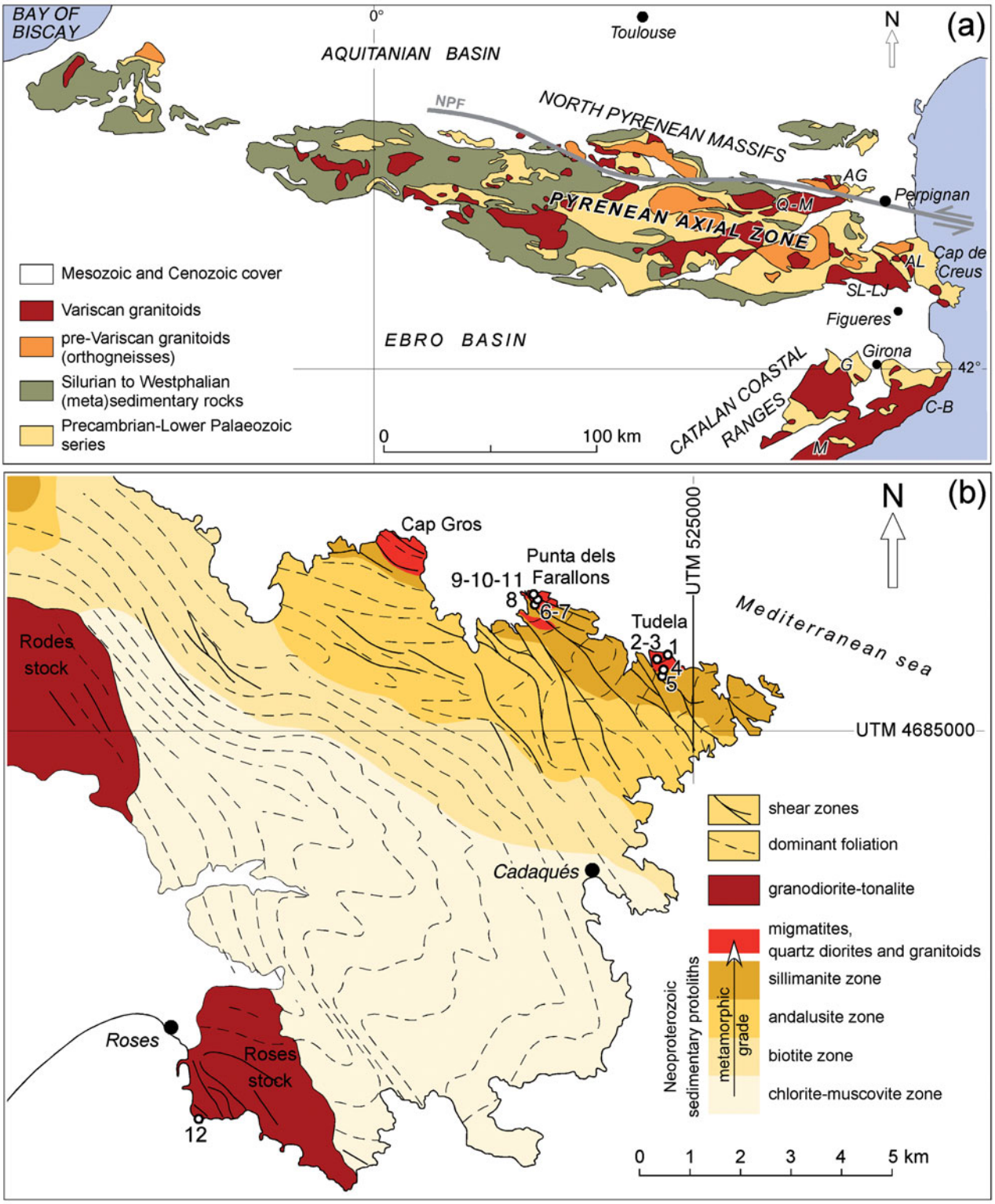

Figure 1. (Colour online) Geological setting of Cap de Creus peninsula. (a) Schematic geological map of NE Iberia showing pre-Palaeozoic and Palaeozoic rocks cropping out along the Pyrenean Axial Zone, the North Pyrenean massifs and the Catalan Coastal Ranges. AG – Agly; NPF – North Pyrenean fault; Q-M – Querigut-Millàs; SL-LJ – Sant Llorenç – La Jonquera; AL – Albera; G – Guilleries; C-B – Costa Brava; M – Montnegre. (b) Geo-structural sketch of the Cap de Creus peninsula showing the main deformation structures and intrusive bodies. Coordinate system refers to the Universal Transverse Mercator Grid (UTM), zone 31-European Datum 50. Locations of samples analysed in this study for geochronology and whole-rocks chemistry are indicated. For simplicity, samples have been labelled from 1 to 12, which correspond to A811-1 to A811-12 in the main text.

https://doi.org/10.1017/S0016756814000041 Published online by Cambridge University Press

been classically regarded as late to post-tectonic in relation to the main Variscan events (Enrique, 2002). This is corroborated by some geochronological data, such as the ^{40}Ar–^{39}Ar ages of *c*. 291–285 Ma for gabbroic rocks and granitoids of the Montnegre massif in the Catalan Coastal Ranges (Solé *et al.* 2002), or the U–Pb ages *c*. 299–276 Ma range for Maladeta granodiorites in the Central Pyrenees (Pereira *et al.* 2014). On the contrary, most plutons located in the internal zones (Eastern Pyrenees and North Pyrenean massifs) form meso- to catazonal intrusions. This is the case, for instance, for the calc-alkaline granitoids and anatectic leucogranites of the Cap de Creus (Druguet, 2001) and Albera (Vilà *et al.* 2005) massifs in the Eastern Pyrenees, of the North Pyrenean Agly massif (Olivier, Gleizes & Paquette, 2004) and of the northernmost Catalan Coastal Ranges (Martínez, Reche & Iriondo, 2008). These intrusions record a weak to well-marked magmatic foliation, which has been correlated with the Variscan D_2 main tectonometamorphic phase, and are heterogeneously affected by the D_3 retrograde mylonitic bands. These features support the widely accepted interpretation that deep to mid-crustal magmatic and metamorphic activity was associated with the Variscan main dextral transpressive D_2 phase (e.g. Leblanc *et al.* 1996; Gleizes, Leblanc & Bouchez, 1998; Druguet, 2001; Denèle *et al.* 2009). Ages of intrusive rocks from the North and Eastern Pyrenean massifs are relatively older on average than those reported for the more external massifs. The U–Pb ages of the Agly plutons range between *c*. 315 and 304 Ma (Olivier *et al.* 2008) and a U–Pb zircon age of 307 ± 2 Ma was obtained for the granodiorite–tonalites of the Quérigut massif (Roberts *et al.* 2000). According to a recent study by Aguilar *et al.* (2013), the syn-D_2 tonalites from the Sant Llorenç – La Jonquera pluton and the nearby Ceret gabbro-diorites yielded U–Pb zircon ages of *c*. 314–311 Ma and 312–307 Ma, respectively. However, younger ages had been previously obtained for La Jonquera granodiorite by O. Maurel (unpub. Ph.D. thesis, Univ. Montpellier II, 2003), ranging from *c*. 302 Ma (hornblende ^{40}Ar–^{39}Ar method) to 295 ± 7 Ma (U–Pb zircon age).

In this paper, we present the results of a study on zircon geochronology carried out with SHRIMP (Sensitive High Resolution Ion Microprobe) of some representative igneous rocks from the Cap de Creus massif. These precise age determinations are useful for dating the complex, crustal-scale tectonic processes responsible for the Cap de Creus structures and the processes of magma generation, emplacement and migmatization associated with deformation, and are significant in terms of reconstructing the geodynamic evolution of the Variscan basement of the Pyrenees.

2. Geological overview of the Cap de Creus massif

The main lithological units present in this massif are a psammitic-pelitic metasedimentary sequence showing a NNE-directed increase in metamorphic grade, and two broad groups of intrusive rocks that are discriminated on the basis of the emplacement level, volume of intrusions and differences in composition (Fig. 1b).

2.a. Metasedimentary rocks

The psammitic-pelitic metasedimentary sequence is formed by two differentiated series, the Lower (Cadaqués) series, which occupies the largest part of the Cap de Creus peninsula, and the overlying Upper (Norfeu) siliciclastic–carbonate series, mainly present towards the south of the peninsula (Carreras & Druguet, 2013). The Lower series consists of alternating greywackes and pelites with minor plagioclase-amphibole rocks, quartzites, calc-silicate rocks and interbedded igneous bodies. A Neoproterozoic age (Ediacaran) is assumed for the sedimentary protoliths of the Lower series on the basis of the age of intrusive porphyries (El Port de la Selva gneisses) dated at *c*. 580–540 Ma by Castiñeiras *et al.* (2008) and by correlation with similar sedimentary sequences of the Iberian Massif. Particular lithological affinities are observed between (i) the plagioclase-amphibole rocks interbedded in the Lower series and some volcanic intercalations in the Villalba series from Galicia (R. Capdevila, unpub. Ph.D. thesis, Univ. Montpellier, 1969), (ii) the interbedded quartzites and those from the Serie Negra of the Ossa–Morena zone, the latter having a maximum depositional age ranging between *c*. 575 and 545 Ma (Schäffer *et al.* 1993; Linnemann *et al*. 2008; Pereira *et al*. 2008, 2012*b*), and (iii) the Cap de Creus Lower and Upper series and, respectively, the Ediacaran to Cambrian rocks of the Lower and Upper units of the Schist-Greywacke Complex from the Iberian Massif (Pereira *et al.* 2012*a*; Talavera *et al*. 2012).

All these metasedimentary rocks were affected by a low-pressure regional metamorphism, characterized in this area by a high thermal gradient (up to 80 °C km^{-1}), with metamorphic grade increasing from the SSW to NNE, from greenschists to upper-amphibolite facies at 670 °C and 470 MPa and local anatexis. According to Druguet (2001), the high thermal gradient was caused by contemporaneous transpressional deformation (D_2 event) and magmatic activity, with domains of high-grade metamorphic rocks and high-D_2 strain coinciding in space and time. This LP–HT metamorphic event would have been preceded by a medium-pressure event at an earlier D_1 orogenic stage, as indicated by the local presence of relics of staurolite in cordierite schists. A retrograde metamorphism (greenschist facies), uniform in grade but strongly inhomogeneous in distribution, developed preferentially along mylonitic zones associated with late D_3 shear zones (Carreras, 2001; Druguet, Alsop & Carreras, 2009).

2.b. The intrusions in the migmatite complexes and the pegmatite dyke swarm

In the high-strain and high-grade metamorphic zone at the north of the massif, small dismembered bodies

https://doi.org/10.1017/S0016756814000041 Published online by Cambridge University Press

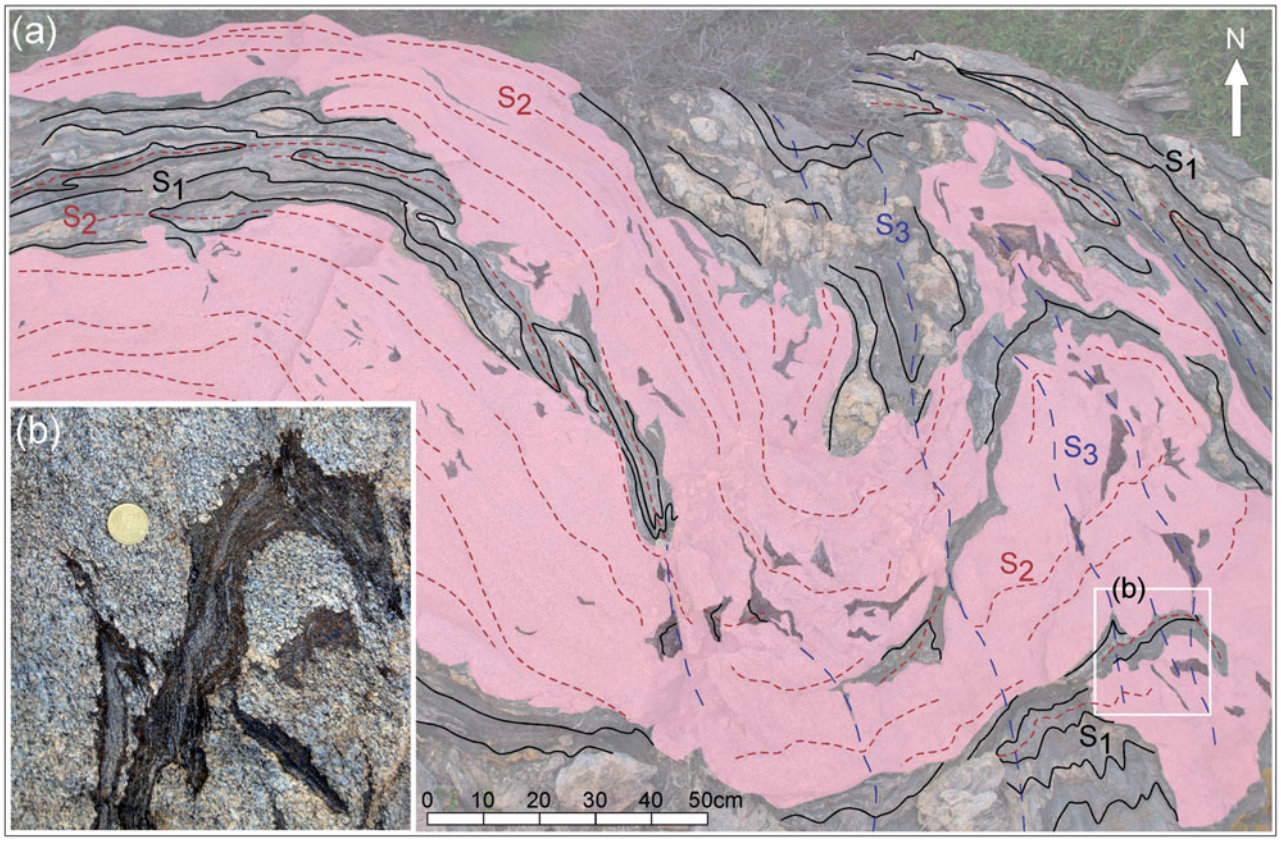

Figure 2. (Colour online) (a) Outlined photograph showing the field relationships between deformed migmatitic schists and intrusive rocks (tonalite-granodiorite) from the Punta dels Farallons migmatite complex. Notice that the granitoid body cross-cuts the D_2 folds, but that both granitoid and migmatites have been progressively folded and foliated (D_2 and D_3) after granitoid intrusion. (b) Detail photograph from the lower right corner of (a). Xenoliths of the migmatitic host, preferentially the melanosome parts, are abundant within the intrusion.

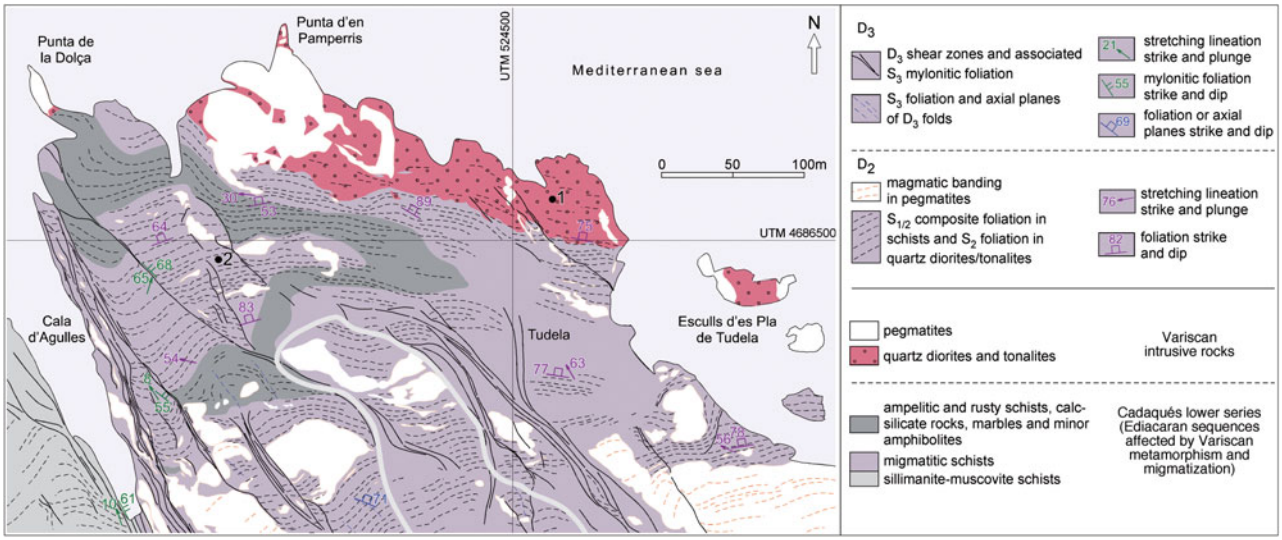

Figure 3. (Colour online) Geological map of the Tudela migmatite complex. Locations of samples from this area analysed for geochronology are indicated. Coordinate system refers to the Universal Transverse Mercator Grid (UTM), zone 31-European Datum 50.

of intrusive quartz gabbros, quartz diorites and granitoids are surrounded by migmatitic schists, altogether forming three migmatite complexes, which are from NW to SE Cap Gros, Punta dels Farallons and Tudela (E. Druguet, unpub. Ph.D. thesis, Univ. Autònoma de Barcelona, 1997; Fig. 1b). The migmatite complexes consist of strongly deformed partially migmatized sillimanite schists, which are intruded by small heterogeneous bodies of quartz gabbros, quartz diorites and granitoids (see the outcrop-scale examples in Fig. 2 and the map and photographs of rocks from the Tudela complex in Figs 3 and 4, respectively).

https://doi.org/10.1017/S0016756814000041 Published online by Cambridge University Press

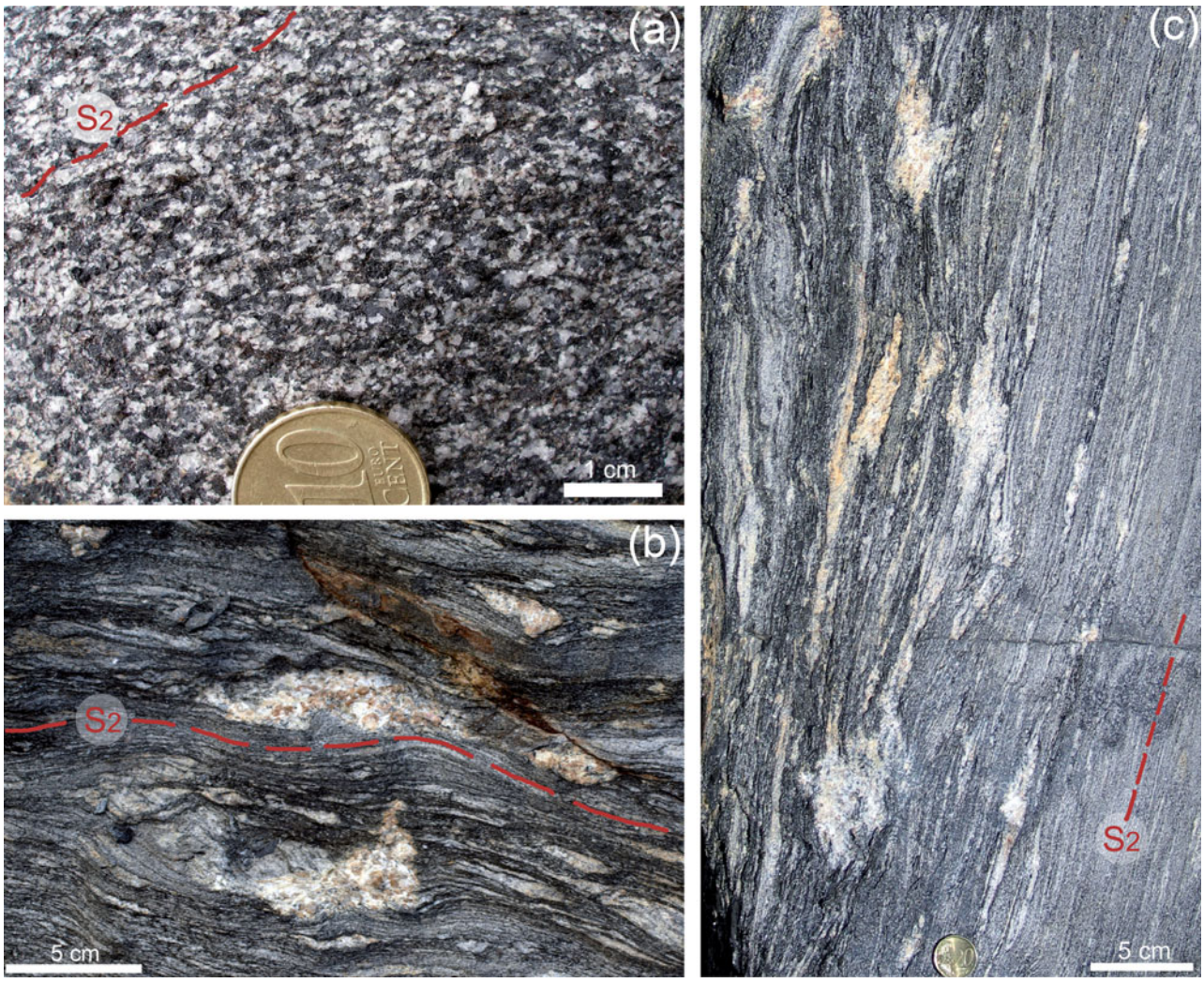

Figure 4. (Colour online) Field photographs of rocks from the Tudela migmatite complex. (a) Quartz diorite with a well-defined magmatic to high-temperature solid state S_2 fabric. Photograph taken next to sample A811-1. (b, c) Patches of syn-D_2 leucosome in strongly deformed migmatitic schists. Photographs taken next to samples A811-1 and A811-2, on sub-horizontal (b) and sub-vertical (c) surfaces.

The plutonic rocks emplaced into the migmatite complexes have been divided into two associations (Druguet, Enrique & Galán, 1995), which are, ordered by relative age of emplacement from older to younger: a mantle-derived calc-alkaline association that includes quartz gabbros, quartz diorites, tonalites, granodiorites and granites, and a peraluminous association that comprises two-mica leucogranites and pegmatites. Rocks from both associations may contain almandine-rich garnet. Garnet may appear in the migmatites as a metamorphic peritectic phase associated with dehydration partial melting of the metasedimentary sequences. It also can be present in intrusive granitoids and quartz diorites. In places, generally adjacent to the migmatitic host rocks, garnet cumulates with more than 60 vol. % garnet are present.

The pegmatites form a dyke swarm that extends farther south to the cordierite-andalusite zone. The absence of large granite intrusion in the area contrasts with the abundance of pegmatite bodies, normally interpreted as late products after granite magma consolidation. In this case, an association between zones of high-grade metamorphism and pegmatite intrusion is suggested according to field relations. It can be inferred that the increase in temperature, and possibly release of fluids, associated with the emplacement of the basic-intermediate wet magmas induced local anatexis, which is the reason for migmatites being restricted to small areas around the intrusions. Furthermore, more extensive anatexis at deeper levels could have generated the peraluminous melts, which can be subsequently emplaced in the perianatectic domain, forming the later association, i.e. leucogranites and the pegmatite dyke swarm. Thus, this later association is likely derived from partial melting of the peraluminous host (Druguet, Enrique & Galán, 1995; Druguet & Hutton, 1998). This interpretation is in accordance with that made by Damm *et al.* (1992), based on H- and O-isotopic signatures, and with that by Autran, Fonteilles & Guitard (1970) for the whole peraluminous leucogranite suite in the Pyrenean Axial Zone. However, an origin by fractionation of a granitoid magma is postulated by other authors

https://doi.org/10.1017/S0016756814000041 Published online by Cambridge University Press

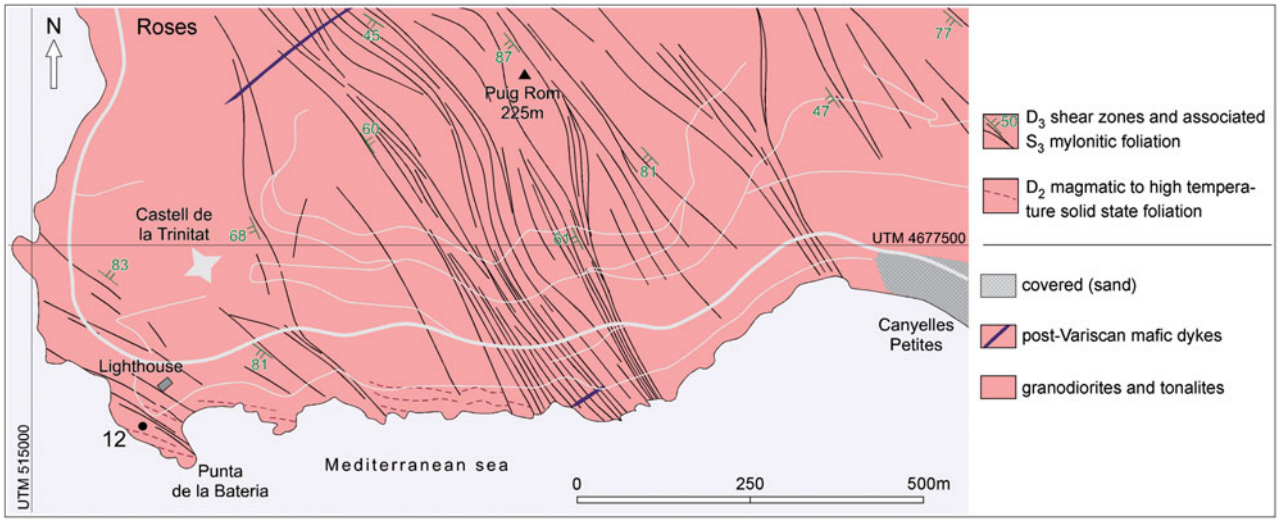

Figure 5. (Colour online) Geological map of the western part of the Roses pluton around the Roses Lighthouse (modified from Carreras *et al.* 2004, fig. 2). Location of sample A811-12 analysed for geochronology is indicated. Coordinate system refers to the Universal Transverse Mercator Grid (UTM), zone 31-European Datum 50.

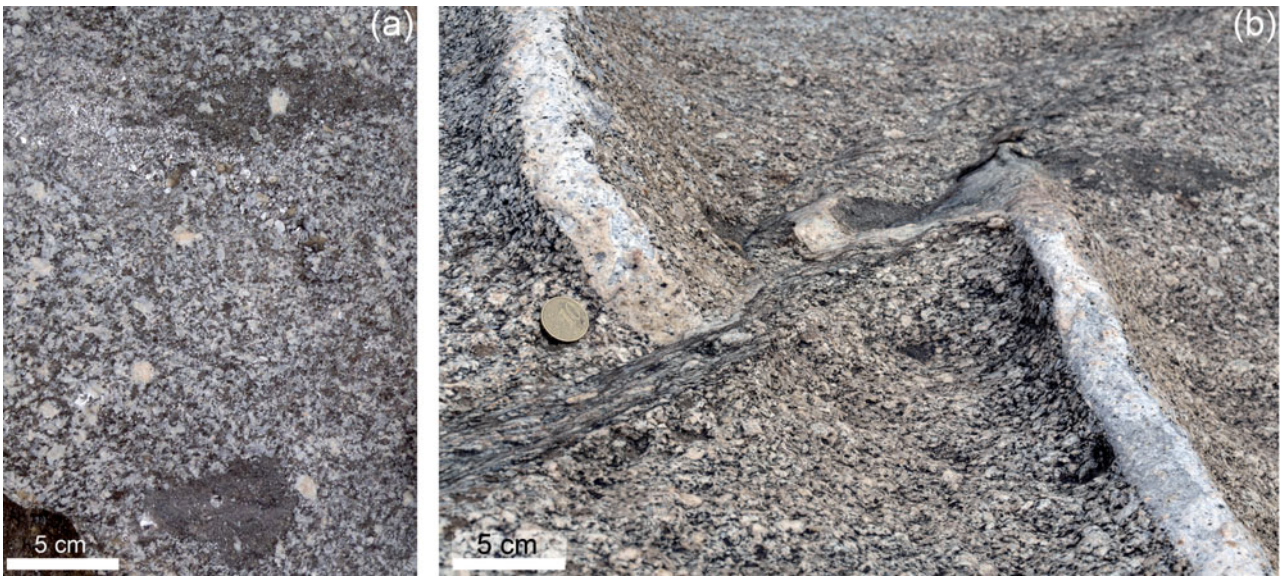

Figure 6. (Colour online) Field photographs of magmatic rocks from the Roses pluton. (a) Hornblende-biotite granodiorite including elongate enclaves of quartz diorite which define the D_2 fabric. Photograph taken next to sample A811-12. (b) Cross-cutting and structural relationships between the syn-D_2 granodiorite, a late-D_2 leucogranite dyke and a D_3 sinistral shear zone. The apparent sinistral movement is due to local Alpine overturning which caused originally NE-dipping dextral shear zones to appear in the Roses area as sinistral ones (Carreras, 2001).

based on mineral compositional trends (Alfonso *et al.* 2003).

2.c. The Roses and Rodes plutons

Two granitoid plutons, the Roses and Rodes, are located south and southwest of the Cap de Creus peninsula, respectively (Figs 1b, 5; Carreras & Losantos, 1982; Carreras *et al.* 2004). They have a rather homogeneous composition of calc-alkaline affinity, varying between granodiorite and tonalite, and are locally rich in microgranular mafic (dioritic) enclaves (Fig. 6). Both are sheet-shaped bodies that clearly correspond to shallow intrusions into low-grade zones of the host metasedimentary sequence. They display a magmatic to high-temperature solid-state fabric (S_2, Fig. 6a), which evolves to a low-temperature, mylonitic foliation (S_3, Fig. 6b) associated with a late anastomosing pattern of shear zones (Fig. 5). The observed continuous gradation of structures suggests a progressive evolution form D_2 to D_3. Aplitic (leucogranite) dykes are abundant in the Roses intrusive body and represent the last differentiates of the pluton, emplaced at the latest cooling stages but prior to D_3 shear zones (Fig. 6b). The whole tectonic history has been interpreted as a result of progressive deformation during cooling (Carreras *et al.* 2004). According to the mentioned features, they are similar to other calc-alkaline granitoid stocks and

https://doi.org/10.1017/S0016756814000041 Published online by Cambridge University Press

batholiths of the basement of the Pyrenees (Gleizes, Leblanc & Bouchez, 1997).

2.d. Tectonics

Three main deformational events have been distinguished in the Cap de Creus. The early event (D_1) developed a penetrative, originally shallow-dipping, S_1 schistosity. Afterwards, a sequence of regional deformation events caused steep structures. S_1 was already moderately to steeply dipping at the onset of D_2, so that a pre-D_2 half-dome-shaped macrostructure is inferred (E. Druguet, unpub. Ph.D. thesis, Univ. Autònoma de Barcelona, 1997).

D_2 was a dextral transpressional event with associated NNW–SSE-directed maximum shortening, producing sub-vertical, NE–SW- to E–W-trending fold axial surfaces affecting bedding/S_1 foliation in prograde metamorphic conditions. D_2 deformation was rather heterogeneous, with zones of high strain preferentially localized in the north and associated with migmatization and granitoid emplacement, taking place around the time of amphibolite-facies peak metamorphism (Druguet, 2001). In the migmatite complexes, migmatites and the syn-D_2 diorites and granitoids of the calc-alkaline association are clearly more deformed (Figs 2, 4) than those belonging to the later peraluminous association (leucogranites and pegmatites), as reported in detail in Druguet & Hutton (1998). This latest association, presumably anatectic in origin, has been interpreted as late-D_2.

Progressive dextral transpression and continuous uplift of the zone produced NW–SE-trending D_3 folds and shear zones at retrograding greenschist-facies conditions (Figs 1–3, 5, 6). This shearing event affected all basement rocks and gave rise to the northern and southern mylonite belts (Fig. 1; Carreras, 2001). As previously summarized in Section 2.c above, the progressive character of deformation from D_2 to D_3 events is particularly well revealed at the Roses pluton (Figs 5, 6; Carreras *et al.* 2004).

3. Whole-rock compositions

Eleven samples from the northern Cap de Creus migmatite complexes (A811-1 to A811-11) and one sample from the Roses granodiorite (A811-12) were initially collected for this study. Whole-rock compositions are listed in Table 1 (see Fig. 1 for sample locations). Sampling was aimed at getting representative rocks of the massif for zircon separation and geochemical characterization. The intrusive suite, which is located within the migmatite complexes, is formed by quartz gabbros, quartz diorites, tonalites and granodiorites and has marked calc-alkaline signatures with anomalous Al-enrichment (Fig. 7). By contrast, the Roses granodiorite (R in Fig. 7), which is located far from the anatectic domains, is close to the metaluminous field and plots together with other intrusive rocks of calc-alkaline affinity of the region. Some leucosomes are relatively rich in CaO and they plot in the field of granodiorites and monzogranites in the O'Connor diagram (Fig. 7b).

With regard to trace elements, quartz diorites associated with the migmatite complexes are characterized by depletions in Nb (< 20 ppm) and Ta (< 2 ppm) (Table 1). Compared to continental andesites (Kelemen, Hanghøj & Greene, 2003), there is a depletion in Sr in all analysed rocks (Fig. 8a). There is a significant enrichment in rare earth elements (REEs), Y, Zr, Pb and Th of the garnet-bearing granodiorites and quartz diorite. Migmatites and leucosomes are almost identical in terms of immobile trace elements. Leucogranites show depletion in incompatible elements (mostly in REEs, Y and Zr) with respect to migmatites and leucosomes. The analysed pegmatite shows strong depletion in all elements with the exception of Rb, Pb and U. Quartz diorites show trace element contents similar to continental andesites used as a reference for normalization (Fig. 8a). However, a slight enrichment in heavy REEs (HREEs) is observed. Figure 8b, c shows chondrite-normalized REE patterns of the analysed samples. Quartz diorites show little fractionation of LREEs/HREEs, with $La_N/Yb_N < 10$ and no Eu anomaly. Similar patterns are shown by the Roses granodiorite and the garnet-rich contaminated quartz diorite and granodiorite rocks collected from an area of intense interaction and mingling between intrusive diorite magmas and a partially molten peraluminous host in the Punta dels Farallons migmatite complex (close to the locality of Fig. 2). Note the steep pattern of migmatites with $La_N/Yb_N > 20$ and no Eu anomaly.

4. Zircon geochronology

4.a. Sample preparation and analytical methods

Four of the samples collected from Cap de Creus were analysed for U, Th and Pb isotopes on the SHRIMP Beijing Centre ion microprobe using a procedure similar to Williams & Claesson (1987) (locations shown in Figs 1b, 3, 5): a quartz diorite (sample A811-1) and a leucosome pod in mica-schists (sample A811-2), both from the Tudela migmatite complex; and a migmatite from the Punta dels Farallons migmatite complex (sample A811-10) and a granodiorite from the Roses pluton (sample A811-12).

Zircon grains were extracted and mounted in epoxy resin with zircon standards SL13 (U = 238 ppm) and TEMORA ($^{206}Pb^*/^{238}U = 0.06683$). The polished mount was photographed and then imaged by scanning electron microscope (SEM) cathodoluminescence (CL) to document the internal growth zoning of the grains (Figs 9, 10) prior to isotope analysis.

The plotted and tabulated analytical uncertainties (Table 2) are 1σ precision estimates. Uncertainties in the calculated mean ages are 95% confidence limits (c.l.) (ts, where t is the Student's t-test multiplier) and, for the mean ^{206}Pb–^{238}U ages, include the uncertainty in the Pb/U calibration (*c.* 0.3–0.5%). Ages were

https://doi.org/10.1017/S0016756814000041 Published online by Cambridge University Press

Table 1. Whole-rock compositions of intrusive rocks and migmatites of the Cap de Creus area

Sample	A811-11	A811-1	A811-7	A811-6	A811-8	A811-12	A811-10	A811-9	A811-5	A811-4	A811-3	A811-2
Rock type*	Qtz-D	Qtz-D	Qtz-D	Grt-Qtz-D	Grt-GD	GD	MGM	LG	PG	LS	LS	LS
SiO_2	52.66	58.39	57.14	55.45	64.88	63.03	71.93	75.68	74.56	70.67	64.03	69.16
TiO_2	1.96	1.28	1.18	1.12	0.25	0.73	0.66	0.11	0.03	0.39	0.66	0.52
$A_{l2}O_3$	18.86	17.99	19.8	17.94	17.69	16.46	12.07	14.76	15.03	15	16.22	14.75
FeOt	10.91	8.57	8.16	9.91	5.91	6.53	6.04	1.34	1.22	3.76	7.41	5.49
MgO	2.85	3.44	1.78	3.89	0.44	1.94	2.25	0.22	0.09	1.07	2.88	2.08
MnO	0.165	0.111	0.067	0.168	0.135	0.092	0.076	0.019	0.044	0.046	0.099	0.093
CaO	6.73	5.75	4.64	4.50	1.50	4.60	1.42	0.82	0.35	1.38	1.69	2.02
Na_2O	3.01	2.38	3.24	2.19	2.89	2.74	1.97	2.72	3.62	2.64	2.21	2.59
K_2O	1.97	1.88	3.29	3.21	5.82	2.98	2.53	2.85	3.94	3.69	3.52	2.51
P_2O_5	0.296	0.293	0.400	0.667	0.157	0.179	0.131	0.128	0.230	0.215	0.172	0.199
Loi	0.80	1.11	0.53	1.10	0.54	0.92	0.56	0.54	0.31	0.77	1.02	0.73
Total	100.2	101.2	100.2	100.1	100.2	100.2	99.6	99.2	99.4	99.6	99.9	100.1
Trace elements (ppm)												
Li	34.30	41.64	55.02	46.99	19.87	29.34	27.46	18.63	39.83	19.63	50.83	35.65
Be	1.90	1.49	1.87	1.76	1.79	2.07	1.00	0.88	1.22	2.19	3.68	1.86
Sc	29.36	20.40	17.71	23.55	16.00	18.32	11.67	6.97	2.28	7.83	15.71	11.20
V	197.20	169.57	66.70	177.00	30.06	105.40	115.00	28.77	31.15	76.75	126.05	97.78
Cr	192.4	314.7	162.8	272.2	229.7	283.1	418.2	259.2	336.4	354.5	327.1	324.3
Co	18.67	17.43	11.07	21.88	3.76	11.33	13.40	1.59	0.75	7.61	17.70	12.70
Ni	9.28	29.60	13.74	35.70	15.33	15.97	45.47	11.01	12.61	26.26	51.69	39.12
Cu	16.43	23.17	17.82	42.66	52.35	12.51	25.26	6.05	7.19	27.95	90.65	15.31
Zn	96.24	98.45	91.35	97.17	61.84	73.89	67.94	20.69	8.74	49.94	89.96	63.24
Ga	23.10	20.00	26.26	21.08	23.76	20.35	15.41	19.53	17.45	16.00	21.12	16.90
Rb	77.72	62.96	129.30	120.10	136.20	116.28	91.03	66.36	154.00	78.55	135.80	93.15
Sr	347.70	331.70	361.00	211.90	256.00	199.83	130.10	73.72	13.92	222.20	185.50	261.00
Y	43.89	20.90	25.04	28.88	75.52	32.33	10.98	5.38	3.73	9.22	12.66	11.66
Zr	205.3	170.9	862.8	223.8	407.5	219.8	205.5	46.6	34.2	111.7	154.5	134.1
Nb	16.20	10.93	17.06	11.56	14.28	12.29	10.33	8.49	8.94	7.66	12.32	9.76
Cs	4.85	3.53	4.68	5.52	2.19	3.21	2.92	0.99	4.31	3.17	4.48	3.21
Ba	564.1	655.2	2325.0	566.5	4805.0	581.2	467.4	435.5	33.4	1356.0	737.0	963.4
La	27.46	24.56	18.66	21.60	147.10	28.38	30.06	7.88	3.32	18.02	35.29	26.48
Ce	65.92	52.20	40.34	47.99	279.90	58.34	62.43	15.69	6.66	38.46	70.40	53.33
Pr	9.11	6.58	5.44	6.11	32.17	7.13	7.18	1.84	0.79	4.45	8.13	6.18
Nd	38.71	25.95	23.50	24.35	116.30	27.82	26.35	6.59	2.55	16.65	29.98	22.77
Sm	8.90	5.36	5.39	5.65	18.63	6.51	5.30	1.52	0.66	3.46	5.87	4.62
Eu	2.19	1.49	2.10	1.64	1.76	1.16	1.20	0.49	0.08	1.08	1.14	1.14
Gd	8.24	4.62	4.94	5.35	15.20	5.86	4.02	1.29	0.53	2.69	4.45	3.61
Tb	1.39	0.73	0.77	0.93	2.51	1.00	0.57	0.21	0.08	0.40	0.65	0.55
Dy	7.79	3.83	4.23	5.16	13.82	5.76	2.62	1.08	0.49	2.03	2.96	2.6
Ho	1.70	0.78	0.94	1.06	3.24	1.22	0.42	0.16	0.09	0.34	0.50	0.44
Er	4.26	1.92	2.72	2.62	8.48	3.05	0.89	0.37	0.31	0.79	1.09	0.96
Tm	0.65	0.29	0.47	0.41	1.38	0.44	0.12	0.06	0.05	0.11	0.14	0.13
Yb	3.94	1.77	2.92	2.55	8.83	2.69	0.69	0.39	0.45	0.69	0.82	0.82
Lu	0.55	0.26	0.39	0.37	1.25	0.38	0.10	0.06	0.08	0.10	0.11	0.11
Hf	0.80	0.13	0.20	0.20	0.31	0.39	0.05	0.26	0.44	0.05	0.06	0.06
Ta	1.04	0.83	0.84	0.92	0.91	0.89	0.71	0.38	0.85	0.95	1.00	0.93
Pb	12.08	14.26	18.72	18.16	44.55	15.59	18.38	33.16	20.11	31.96	23.38	23.00
Th	4.16	7.16	1.87	3.38	58.87	9.07	11.49	3.03	1.02	5.30	14.7	10.38
U	1.38	1.63	1.34	1.95	3.83	2.29	1.55	3.51	2.59	2.25	2.56	1.91

*Qtz-D – quartz diorite; Grt-Qtz-D – garnet-quartz diorite; Grt-GD – garnet granodiorite; GD – granodiorite; MGM – migmatite; LG – leucogranite; PG – pegmatite; LS – leucosomes.

calculated using the constants recommended by the IUGS Subcommission on Geochronology (Steiger & Jäger, 1977). Common Pb corrections assumed a model common Pb composition appropriate to the age of each spot (Cumming & Richards, 1975). Best estimates of the individual ages (inferred ages, Table 2) were calculated from the radiogenic $^{207}Pb/^{206}Pb$ (common Pb correction based on ^{204}Pb) for discordant zircons and zircons older than 1.5 Ga, and from the radiogenic $^{206}Pb/^{238}U$ (common Pb correction based on ^{207}Pb) for concordant younger zircons. In a few cases, the analyses tabulated and plotted were corrected for common Pb using ^{208}Pb, meaning that radiogenic $^{208}Pb/^{206}Pb$ and $^{208}Pb/^{232}Th$ were not independently determined.

4.b. SHRIMP U–Th–Pb results

The results of the zircon U–Th–Pb analyses are listed in Table 2 and plotted on concordia diagrams in Figures 9 and 10. A detailed description of the analysed samples for zircon geochronology and a summarized report of the ages are given below.

4.b.1. Quartz diorite from the Tudela migmatite complex

Sample A811-1 is from a medium-grained quartz diorite with quartz + plagioclase + hornblende + biotite ± K-feldspar, and zircon, apatite, tourmaline and opaque minerals as accessory phases. The sample was

https://doi.org/10.1017/S0016756814000041 Published online by Cambridge University Press

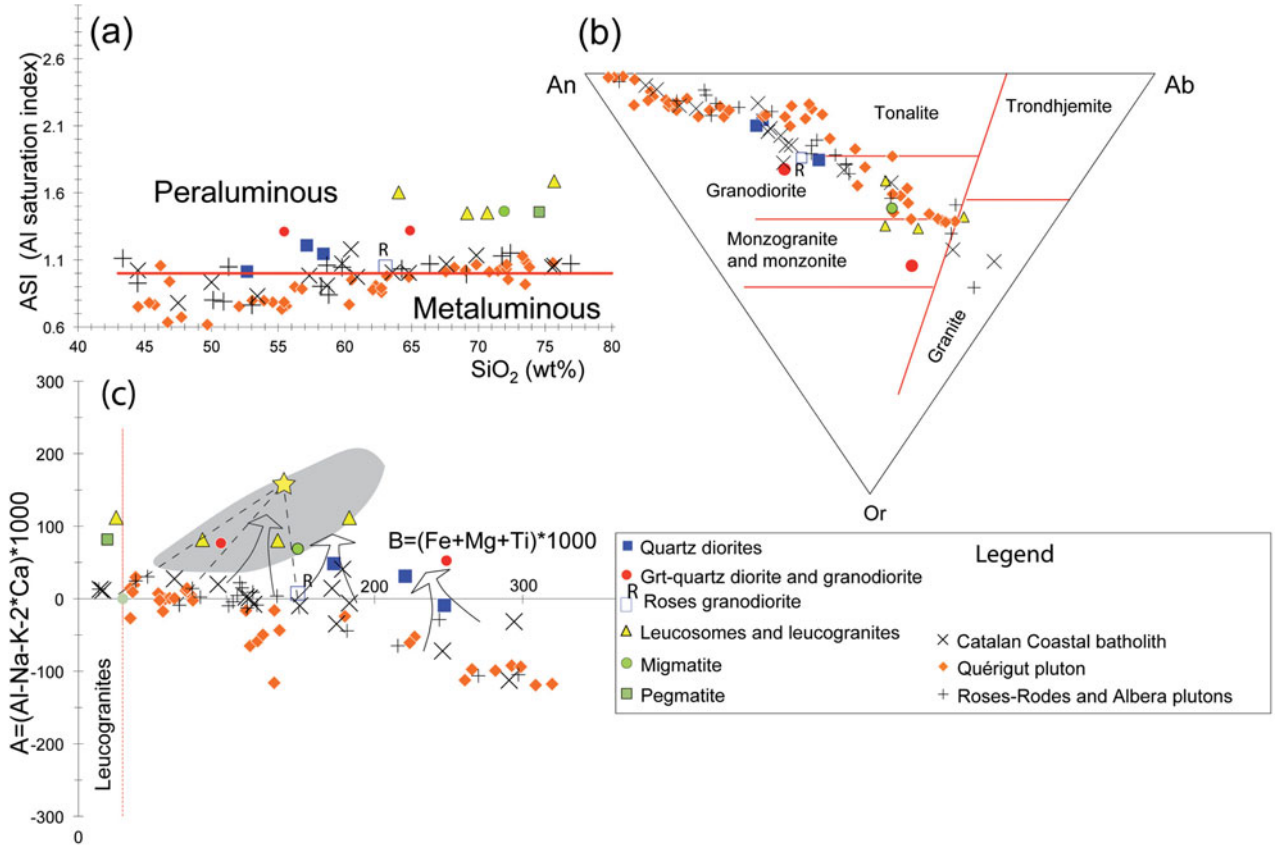

Figure 7. (Colour online) Geochemical diagrams plotting intrusive rocks and migmatites of the Cap de Creus area. (a) Alumina saturation index (ASI = molar Al/((Ca-1.67*P) + Na + K)) against SiO_2 showing the anomalous composition of some diorites and garnet-bearing granodiorites, which plot in the peraluminous field. (b) O'Connor feldspar classification diagram (Ab – albite; An – anorthite; Or – orthoclase). (c) The A–B diagram (De la Roche, 1978; Debon & Le Fort, 1983) showing the area of Iberian Neoproterozoic greywackes and average of pelitic rocks (yellow star) according to data compilation in Fernández *et al.* (2008). For comparison, regional data from granitoid plutons of the Pyrenees (Quérigut: Roberts *et al.* 2000; Albera: Vilà *et al.* 2005; Rodes–Roses: Debon, Enrique & Autran, 1995) and from the Catalan Coastal ranges (Enrique, 1990) are shown. The large arrows in (c) indicate the shift of 'normal' calc-alkaline compositions (cafemic series of Debon & Le Fort, 1983) towards the area of the metasedimentary (peraluminous) country rocks, where migmatites, leucosomes and anatectic granites are plotted.

collected from a rather homogeneous quartz diorite-tonalite body (*c*. 300 × 50 m of surface size) elongated parallel to the WNE–ESE S_2 foliation and intruded into strongly deformed migmatitic schists (Fig. 3). A magmatic to solid-state foliation is weakly to well-defined by the preferred orientation of amphibole, biotite and plagioclase crystals (Fig. 4a).

The zircon population is very characteristic and morphologically homogeneous (Fig. 9). The medium- to coarse-grained zircons (100–300 μm) are mostly euhedral acicular prismatic grains without inclusions with a few bipyramidal. CL imaging shows that most of the grains have indistinct banded or longitudinal zoning or are unzoned without old cores. The igneous grains have low to moderate uniform U contents (168–387 ppm; average 226 ppm) and moderate, very regular Th/U ratios ranging from 0.4 to 0.59 (average = 0.48) (Table 2), consistent with precipitation from a melt phase of a felsic–intermediate metaluminous source. Considering all analyses performed, discarding two spots that gave discordant ages (Analyses 3.1. and 7.1.; Table 2; Fig. 9), the other seven ^{206}Pb–^{238}U ages are clustered, within analytical uncertainty (MSWD = 0.58, probability = 0.75), and yield a well-defined weighted mean age of 298.8 ± 3.8 Ma (95 % c.l.; Late Carboniferous – Early Permian). This is the best estimate of the crystallization age of the quartz diorite from the Tudela migmatitic complex (Fig. 9).

4.b.2. *Roses granodiorite*

Sample A811-12 is a medium- to coarse-grained granodiorite from the Roses Lighthouse (see location in Fig. 5) composed of quartz, plagioclase, K-feldspar, biotite and hornblende, with zircon as the main accessory phase. A weak magmatic to solid-state foliation is defined by the preferred orientation of plagioclase, mafic minerals and elongate microquartz dioritic enclaves (Fig. 6a). Zircons are morphologically homogenous but very variable in size, including medium- to coarse-grained (100–300 μm) euhedral prismatic grains, with many mineral inclusions. CL imaging shows that most zircons are simple and have a thin concentric growth zoning. In composite grains, the thin concentric zoning surrounds a diffuse zoning or unzoned cores (Fig. 9).

https://doi.org/10.1017/S0016756814000041 Published online by Cambridge University Press

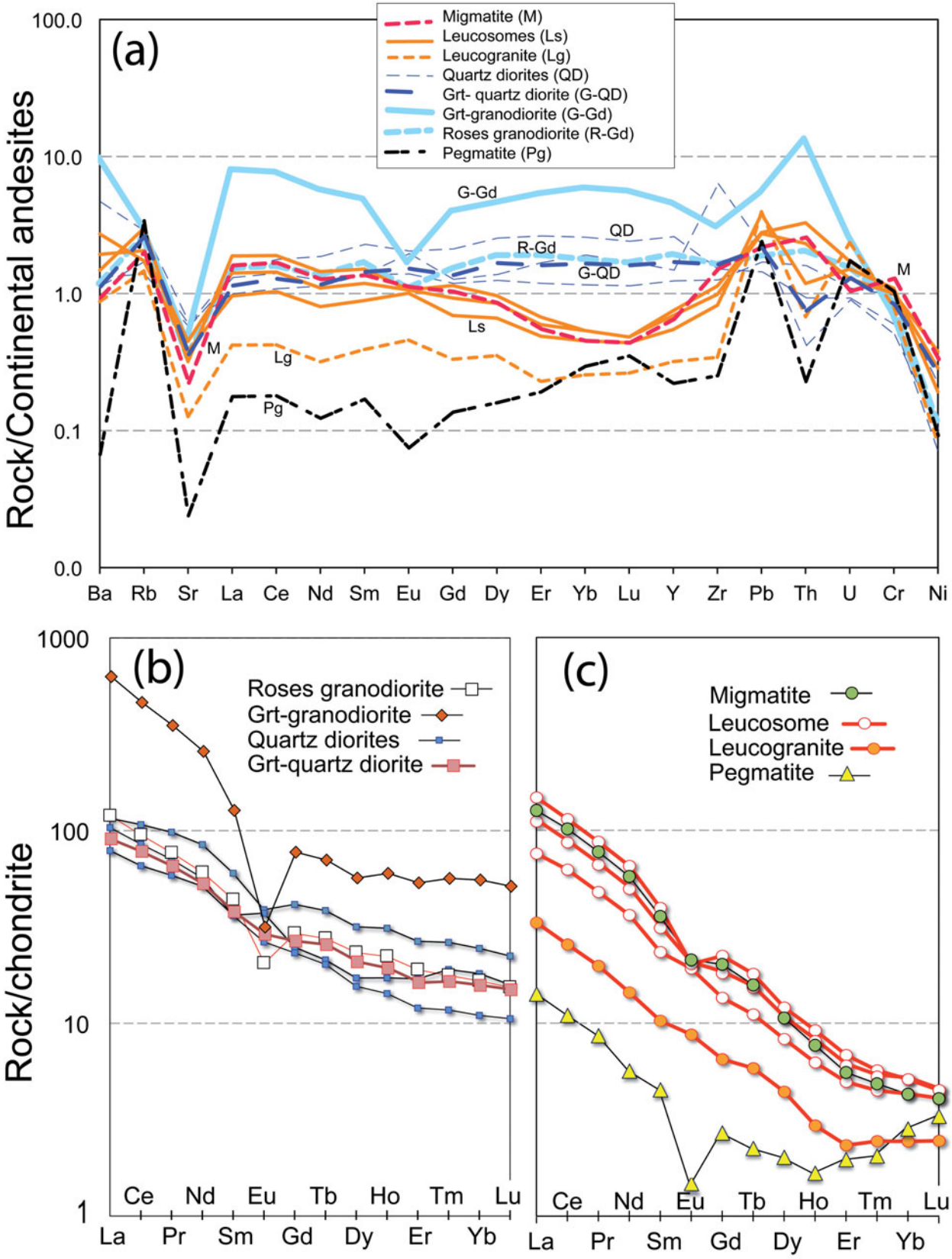

Figure 8. (Colour online) (a) Spider diagram showing relevant trace elements normalized to average continental andesites (Kelemen *et al.* 2003). Note the enrichment in REE in the Grt-granodiorite with respect to other intrusive rocks and the strong depletion in the pegmatite with the exception of Rb, U and Pb. (b) and (c) Chondrite-normalized (Nakamura, 1974) REE abundances of analysed rocks.

https://doi.org/10.1017/S0016756814000041 Published online by Cambridge University Press

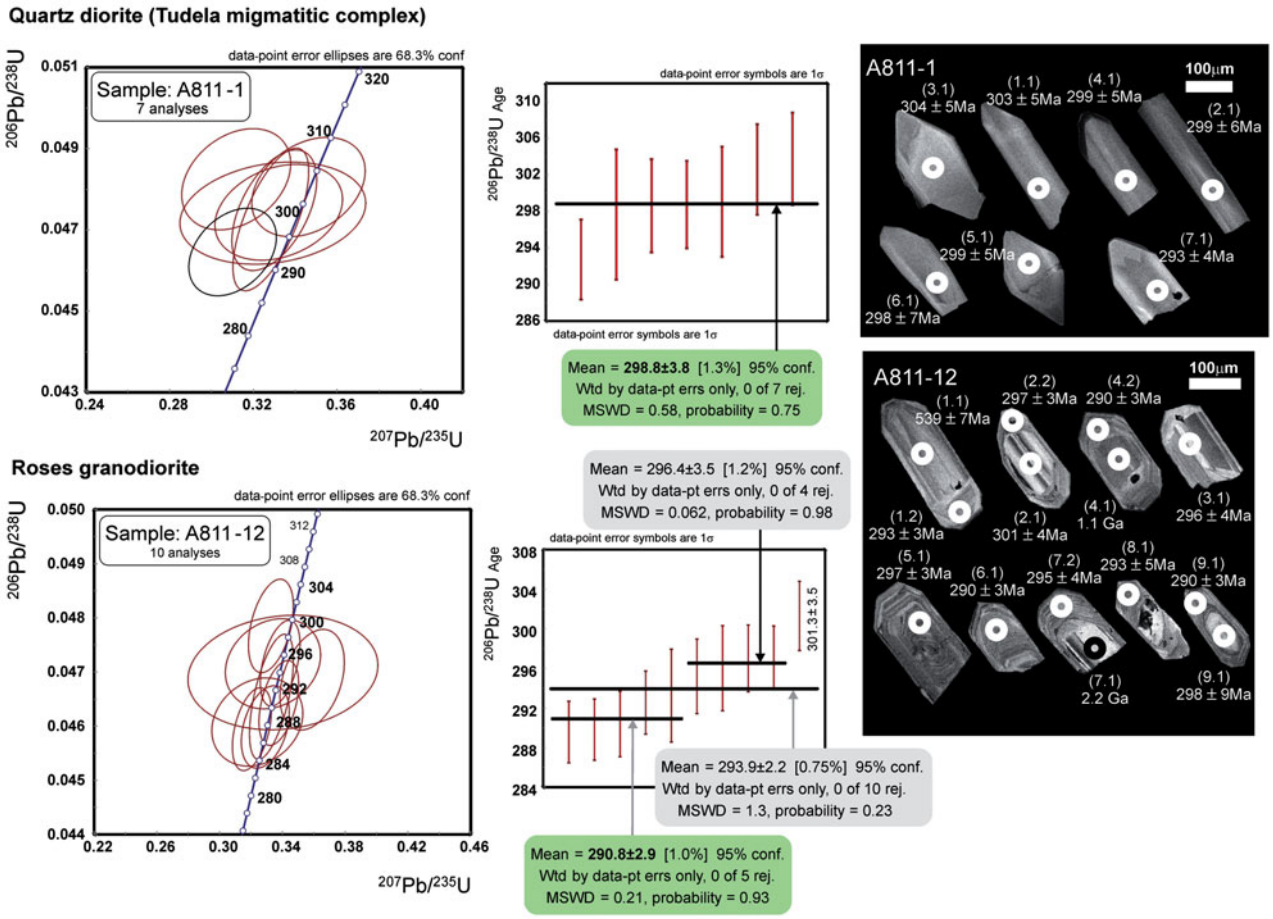

Figure 9. (Colour online) CL imaging of representative zircons with analytical sites, U–Pb concordia, and mean age plots of zircon grains from samples A811-1 (Tudela quartz diorite) and A811-12 (Roses granodiorite).

The majority of the selected zircon grains are composite (grains 1, 2, 4, 7 and 9; Fig. 9) with a core with smooth edges surrounded by a concentric zoned euhedral phase. Some composite grains show cores with longitudinal zoning (grain 2). The obtained U–Pb ages reveal that some of the composite grains have cores much older than the overgrowth (inherited zircon with *c*. 2.2 Ga, Palaeoproterozoic; grain 7), but other grains have cores with ages slightly older than the overgrowth (grains 2 and 9). U–Th–Pb isotopic analyses of 11 not-inherited igneous cores or grains (Table 2) show a range of moderate U contents (168–939 ppm; average = 651 ppm) and moderate Th/U ratios (0.22–1.1; average = 0.40) consistent with precipitation from a melt phase of a felsic–intermediate source.

The U–Pb isotopic compositions of the 11 analyses are similar. Analysis 9.1 is very discordant, probably due to an excess of common lead. The remaining ten analyses can be considered equal within analytical uncertainty (MSWD = 1.3; probability = 0.23), giving a weighted mean ^{206}Pb–^{238}U age of 293.9 ± 2.2 Ma (95 % c.l.; Early Permian). However, the low probability reflects some scattering around that age from 289.6 ± 3.1 Ma to 301.3 ± 3.5 Ma (interval of about 12 Ma). There is no apparent reason to explain this range of ^{206}Pb–^{238}U ages by radiogenic Pb loss, and therefore, this interval of ages could be the effect of the long residence of melts within the magma chamber and more than one stage of zircon crystallization. Grains 2 and 9 have cores with ages slightly older than the overgrowth, separated by *c*. 4–8 Ma. Leaving aside the Analysis 2.2 of a banded zoned core, it is possible to define two age groups (Fig. 9): (i) four analyses equal within analytical uncertainty (MSWD = 0.062; probability = 0.98) yielding a weighted mean ^{206}Pb–^{238}U age of 296.4 ± 3.5 Ma (95 % c.l.), and (ii) five analyses equal within analytical uncertainty (MSWD = 0.21; probability = 0.93) with a weighted mean ^{206}Pb–^{238}U age of 290.8 ± 2.9 Ma (95 % c.l.). The younger Early Permian age is considered the best estimate age of the last stage of crystallization of the Roses granodiorite.

In addition, the cores of three composite zircons (grains 1, 4 and 7) are Cambrian (Analysis 1.1: 539 ± 7 Ma), Mesoproterozoic (Analysis 4.1: 1.1 Ga) and Palaeoproterozoic (Analysis 7.1: 2.2 Ga).

4.b.3. Migmatite from the Punta dels Farallons migmatitic complex

Sample A811-10 is a stromatic migmatite formed by millimetre-thick leucosome lenses alternating with irregular, intricate layers of biotite and sillimanite-rich melanosome and mesosome. The leucosomes are trondhjemitic in composition, mainly composed of

https://doi.org/10.1017/S0016756814000041 Published online by Cambridge University Press

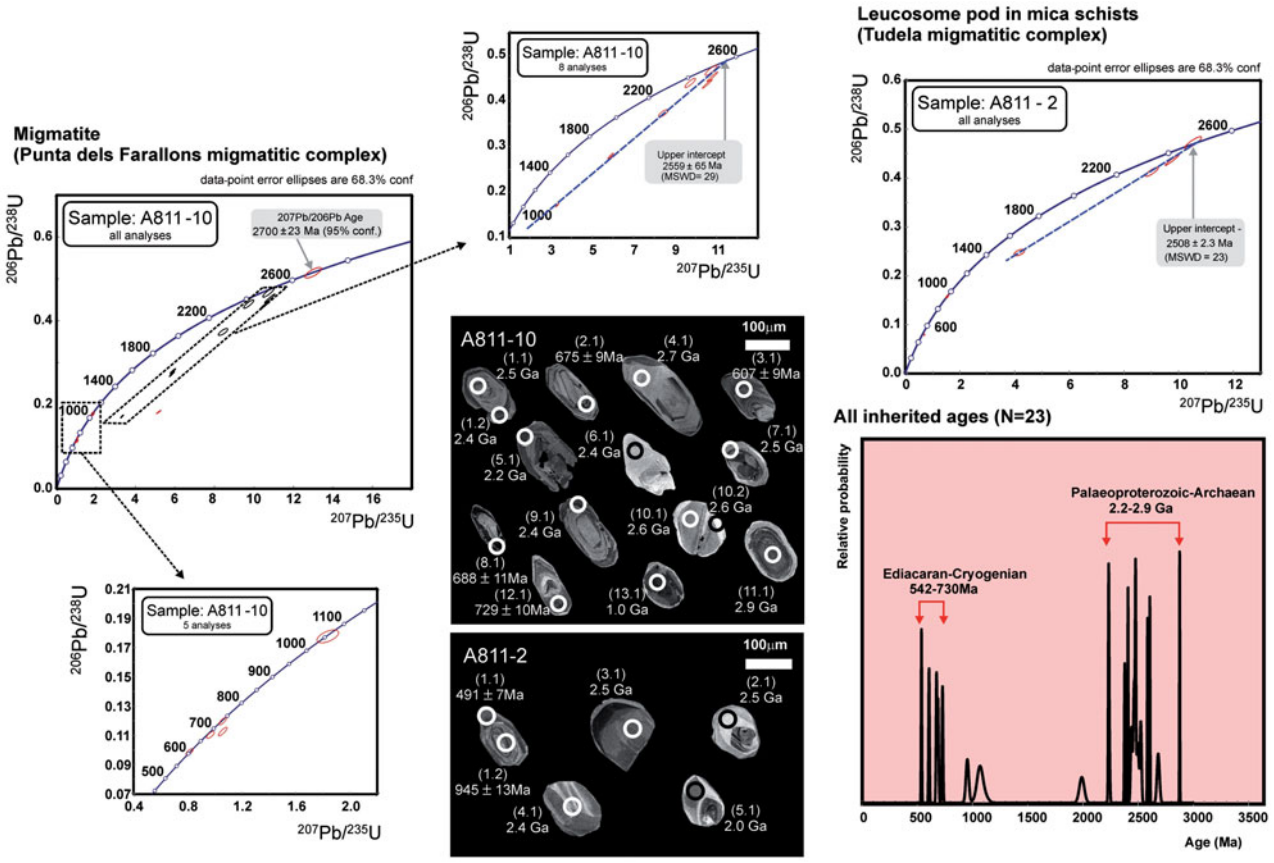

Figure 10. (Colour online) CL imaging of representative zircons with analytical sites, U–Pb concordia, and mean age plots of zircon grains from samples A811-10 (Punta dels Farallons migmatite) and A811-2 (Tudela leucosome), and diagram of relative probability with all the inherited zircons analysed in this study.

quartz and plagioclase, with cordierite and zircon as the main accessory phases. The migmatitic banding is parallel to the main S_2 fabric present in the surrounding igneous and metamorphic rocks.

The majority of the zircons are medium grained (100 to 250 µm diameter), subhedral to anhedral stubby prisms to equant grains. CL imaging revealed an equal quantity of composite and simple grains. Simple grains show an oscillatory concentric zoning (grain 2). The composite zircons have cores with variable internal structures surrounded by faintly concentric zoned or unzoned (low or high luminescent) external growths (grains 1, 7, 9 and 11). An extremely thin, high luminescence external rim (a metamorphic overgrowth or a recrystallization front) is visible in almost all grains but is too thin to be analysed with SHRIMP.

U–Th–Pb isotopic analyses of 15 spots from 13 representative zircon grains are listed in Table 2 and plotted in Figure 10. Most zircons are inherited grains from a metasedimentary source with a remarkable Precambrian population. The obtained U–Pb ages are divided into two groups. A dominant group representative of the Palaeoproterozoic–Neoarchaean boundary includes nine analyses that show U–Pb isotopic compositions distributed along a discordia line, including a very concordant ^{207}Pb–^{206}Pb age of *c*. 2.7 Ga (Analysis 4.1). Excluding the more discordant age (Analysis 11.1 with discordance = 63 %), the remaining eight ages define an improved discordia regression with an upper intercept at 2559 ± 65 Ma (MSWD = 29) (Fig. 10). The remaining older ages fall in the interval *c*. 2.8–2.6 Ga. A second group is formed by scattered and almost Neoproterozoic concordant ^{206}Pb–^{238}U ages (Cryogenian: Analysis 12.1: 729.2 ± 9.7 Ma, Analysis 8.1: 688 ± 11 Ma and Analysis 2.1: 674.8 ± 9.1 Ma; and Ediacaran: Analysis 3.1: 607.2 ± 8.4 Ma).

A single analysis gave a Mesoproterozoic age (Analysis 13.1: 1054 ± 16 Ma). In addition, three external overgrowths with low Th/U ranging from 0.01 to 0.07 (typical of high-grade metamorphic overgrowths) yielded Cryogenian (Analysis 8.1: *c*. 688 Ma and Analysis 12.1: *c*. 729 Ma) and Palaeoproterozoic (Analysis 1.2: *c*. 2.4 Ga) ages (Fig. 10).

4.b.4. Leucosome pod from the Tudela migmatitic complex

Sample A811-2 is from an isolated centimetre-thick leucosome pod confined to metapelitic layers. Leucosomes from this area are typically medium to coarse grained and their composition is leucogranitic to trondhjemitic, with quartz, feldspar and cordierite as the main mineral assemblage. They have a lenticular to irregular, patchy shape, sub-concordant with the S_2 fabric in the host metapelites (Fig. 4b, c), suggesting syn-D_2 partial melting of the relatively more fertile layers (Druguet & Carreras, 2006).

https://doi.org/10.1017/S0016756814000041 Published online by Cambridge University Press

Table 2. Summary of SHRIMP U–Pb zircon data from the Cap de Creus samples

Sample A811-1: Quartz diorite from the Tudela migmatitic complex; coordinates: 42° 19′ 43.71″ N/3° 17′ 47.89″ E

Grain Spot	Structure	% $^{206}Pb_c$	ppm U	ppm Th	$^{232}Th/^{238}U$	Ppm $^{206}Pb^*$	(1) $^{206}Pb/^{238}U$ Age		(1) $^{207}Pb/^{206}Pb$ Age		% Dis-cordant	(1) $^{207}Pb^*/^{206}Pb^*$	±%	(1) $^{207}Pb^*/^{235}U$	±%	(1) $^{206}Pb^*/^{238}U$	±%	err corr
1.1	BZ to UZ	0.40	188	89	0.490	7.80	302.6	± 5.0	297	± 110	− 2	0.0523	4.9	0.346	5.2	20.81	1.7	.325
2.1	BZ	0.68	220	95	0.446	9.05	299.1	± 6.0	214	± 81	− 40	0.0504	3.5	0.330	4.1	21.06	2.1	.509
3.1	UZ	1.06	168	70	0.433	7.02	303.7	± 5.1	43	± 130	− 614	0.0469	5.2	0.312	5.5	20.73	1.7	.309
4.1	BZ	0.91	196	87	0.456	8.07	298.7	± 4.8	231	± 130	− 29	0.0508	5.8	0.332	6.1	21.08	1.6	.271
5.1	UZ	0.83	186	88	0.491	7.63	298.6	± 5.1	212	± 200	− 41	0.0504	8.7	0.329	8.9	21.09	1.7	.196
6.1	UZ	0.30	235	100	0.438	9.56	297.7	± 7.1	213	± 62	− 40	0.0504	2.7	0.328	3.6	21.16	2.5	.674
7.1	BZ to UZ	0.76	387	221	0.590	15.5	292.7	± 4.4	119	± 99	− 146	0.0484	4.2	0.310	4.5	21.53	1.5	.343

Sample A811-12: Roses granodiorite; coordinates: 42° 14′ 43.4″ N/3° 10′ 57.83″ E

Grain Spot	Structure	% $^{206}Pb_c$	ppm U	ppm Th	$^{232}Th/^{238}U$	Ppm $^{206}Pb^*$	(1) $^{206}Pb/^{238}U$ Age		(1) $^{207}Pb/^{206}Pb$ Age		% Dis-cordant	(1) $^{207}Pb^*/^{206}Pb^*$	±%	(1) $^{207}Pb^*/^{235}U$	±%	(1) $^{206}Pb^*/^{238}U$	±%	err corr
1.1	BZC	0.79	270	42	0.161	20.3	538.7	± 6.5	502	± 83	− 7	0.0573	3.8	0.6880	4.0	11.47	1.3	.314
1.2	CZO	0.38	808	150	0.192	32.4	292.6	± 3.2	319	± 50	8	0.0528	2.2	0.3377	2.5	21.54	1.1	.451
2.1	CZO	1.90	596	253	0.439	24.6	297.0	± 3.4	258	± 140	− 15	0.0514	5.9	0.3340	6.0	21.21	1.2	.194
2.2	BZC	0.47	752	228	0.313	31.0	301.3	± 3.5	215	± 60	− 40	0.0504	2.6	0.3327	2.8	20.90	1.2	.419
3.1	BZ	3.28	188	103	0.565	7.85	296.0	± 4.3	309	± 270	4	0.0525	12	0.3400	12.0	21.28	1.5	.127
4.1	BZC to UZC	0.79	91	89	1.011	13.6	1028.0	± 13	1082	± 79	5	0.0755	3.9	1.7990	4.2	5.786	1.4	.339
4.2	CZO	0.36	930	379	0.421	36.9	289.8	± 3.1	282	± 65	− 3	0.0519	2.9	0.3290	3.1	21.75	1.1	.357
5.1	CZ	0.48	939	379	0.417	38.2	297.1	± 3.2	288	± 50	− 3	0.0521	2.2	0.3386	2.5	21.20	1.1	.450
6.1	CZ	0.41	709	264	0.385	28.1	289.6	± 3.1	223	± 53	− 30	0.0506	2.3	0.3206	2.6	21.77	1.1	.430
7.1	BZC	0.23	147	53	0.375	45.9	1998.0	± 20	2237	± 12	11	0.1408	0.72	7.0520	1.4	2.753	1.2	.855
7.2	CZO	0.43	467	141	0.313	18.9	295.2	± 3.8	435	± 79	32	0.0556	3.5	0.3590	3.8	21.34	1.3	.347
8.1	CZO	0.28	785	252	0.332	31.5	293.3	± 4.7	281	± 51	− 4	0.0519	2.2	0.3330	2.8	21.49	1.6	.591
9.1	UZC	14.40	168	117	0.716	8.0	298.0	± 8.5	− 380	± 1500	177	0.0390	56	0.2600	56.0	21.14	2.9	.052
9.2	CZO	0.57	812	254	0.323	32.3	290.4	± 3.3	241	± 130	− 20	0.0510	5.8	0.3240	5.9	21.70	1.2	.197

Table 2. Continued.

Sample A811-10: Migmatite from the Punta dels Farallons migmatitic complex; coordinates: 42° 20′ 24.33″ N/3° 15′ 51.27″ E

Grain Spot	Structure	% $^{206}Pb_c$	ppm U	ppm Th	$^{232}Th/^{238}U$	Ppm $^{206}Pb^*$	(1) $^{206}Pb/^{238}U$ Age		(1) $^{207}Pb/^{206}Pb$ Age		% Dis-cor-dant	(1) $^{207}Pb^*/^{206}Pb^*$	±%	(1) $^{207}Pb^*/^{235}U$	±%	(1) $^{206}Pb^*/^{238}U$	±%	err corr
1.1	CZC	0.18	172	96	0.58	69.1	2473	±32	2524	±14	2	0.16660	0.84	10.740	1.8	0.4675	1.6	.882
1.2	CZO	0.03	950	67	0.07	228	1589	±21	2379	±8.1	33	0.15294	0.47	5.892	1.5	0.2794	1.5	.951
2.1	CZ	0.29	926	529	0.59	88	674.8	±9.1	731	±28	8	0.06367	1.30	0.969	1.9	0.1104	1.4	.732
3.1	CZ	0.20	777	342	0.45	66.1	607.2	±8.4	596	±32	−2	0.05979	1.50	0.814	2.1	0.0988	1.5	.699
4.1	CZ	0.15	183	89	0.50	81.2	2677	±35	2682	±23	0	0.18320	1.40	13.010	2.1	0.5147	1.6	.757
5.1	UZO	0.04	775	151	0.20	114	1019	±13	2233	±7.0	54	0.14047	0.40	3.317	1.5	0.1713	1.4	.961
6.1	HL-UZ	0.11	313	159	0.52	118	2350	±30	2462	±14	5	0.16060	0.85	9.740	1.7	0.4398	1.5	.872
7.1	UZO	0.09	335	44	0.13	107	2044	±25	2497	±19	18	0.16400	1.10	8.440	1.8	0.3732	1.4	.784
8.1	LL-UZO	0.66	1771	59	0.03	173	688	±11	876	±22	21	0.06823	1.10	1.060	2.0	0.1126	1.7	.851
9.1	UZO	0.05	849	79	0.10	199	1553	±19	2408.6	±5.2	36	0.15561	0.31	5.845	1.4	0.2724	1.4	.977
10.1	UZC	0.10	545	69	0.13	205	2340	±28	2606	±5.4	10	0.17499	0.32	10.560	1.5	0.4375	1.4	.976
10.2	HL-UZO	0.01	326	77	0.24	127	2410	±31	2585.4	±6.0	7	0.17284	0.36	10.800	1.6	0.4533	1.5	.974
11.1	WCZC to UZC	0.14	1161	604	0.54	182	1078	±14	2876	±4.4	63	0.20622	0.27	5.174	1.4	0.1820	1.4	.981
12.1	WCZO	0.21	689	9	0.01	71.1	729.2	±9.7	747	±22	2	0.06415	1.00	1.059	1.7	0.1198	1.4	.807
13.1	WCZC	0.44	155	85	0.56	23.8	1054	±16	1066	±48	1	0.07490	2.40	1.835	2.9	0.1776	1.6	.567

Sample A811-2: Leucosome pod in mica-schists from the Tudela migmatitic complex; coordinates: 42° 19′ 42.16″ N/3° 17′ 37.39″ E

Grain Spot	Structure	% $^{206}Pb_c$	ppm U	ppm Th	$^{232}Th/^{238}U$	Ppm $^{206}Pb^*$	(1) $^{206}Pb/^{238}U$ Age		(1) $^{207}Pb/^{206}Pb$ Age		% Dis-cor-dant	(1) $^{207}Pb^*/^{206}Pb^*$	±%	(1) $^{207}Pb^*/^{235}U$	±%	(1) $^{206}Pb^*/^{238}U$	±%	err corr
1.1	UZO	0.14	728	50	0.07	49.6	491	±6.7	741	±21	34	0.0523	4.9	0.346	5.2	0.04806	1.7	.325
1.2	WCZC	0.16	558	232	0.43	75.8	945	±13	954	±26	1	0.0504	3.5	0.330	4.1	0.04748	2.1	.509
2.1	UZC to BZC	0.28	72	25	0.36	29.4	2495	±34	2472	±16	−1	0.0469	5.2	0.312	5.5	0.04825	1.7	.309
3.1	HL-UZO	0.08	338	97	0.30	127.0	2336	±32	2477	±6.6	6	0.0508	5.8	0.332	6.1	0.04743	1.6	.271
4.1	BZ	0.21	218	96	0.46	77.3	2228	±28	2440	±15	9	0.0504	8.7	0.329	8.9	0.04741	1.7	.196
5.1	UZO	1.14	77	85	1.14	16.5	1425	±22	1990	±44	28	0.0504	2.7	0.328	3.6	0.04730	2.5	.674

CZ – concentric zoned; CZC – concentric zoned core; CZO – concentric zoned overgrowth; BZ – banded or longitudinal zoned; BZC - banded or longitudinal zoned core; UZ – unzoned; UZC – unzoned core; UZO – unzoned overgrowth; WCZC – weak concentric zoned core; WCZO – weak concentric zoned overgrowth; LL – low luminescence.; HL – high luminescence.
Errors are 1-sigma; Pb_c and Pb^* indicate the common and radiogenic portions, respectively. Error in Standard calibration was 0.28 % (not included in above errors but required when comparing data from different mounts). (1) Common Pb corrected using measured ^{204}Pb.

The majority of the zircons are medium to coarse grained (130 to 210 μm diameter), anhedral to subhedral bipyramidal prisms (grain 1), equant and rounded grains (grain 2) (Fig. 10). Composite and simple zircons are in equal proportion and their internal zonation varies from thin to wide bands of oscillatory concentric zoning, to parallel banded zoning or unzoned.

In this sample, six U–Th–Pb isotopic analyses on five representative zircon grains were performed (Table 2 and plotted in Fig. 10). The obtained results show that the younger overgrowth (Analysis 1.1) gives a discordant (34 %) ^{206}Pb–^{238}U age of 491 ± 6.7 Ma with a low Th/U = 0.07 and U = 728 ppm, compatible with zircon precipitated from trace-element-rich partial melts, probably representing a relic of high-temperature metamorphism (Williams & Claesson, 1987; Heaman, Bowins & Crocket, 1990). This unzoned pyramidal overgrowth surrounds an older core dated at 945 ± 13 Ma (Tonian). Assuming that the remaining four spots are affected by a progressive radiogenic Pb and Th loss, their U–Pb isotopic compositions distributed along a straight discordia line intercepts the concordia curve at 2508 ± 23 Ma (MSWD = 2.3) (Fig. 10).

5. Discussion

Intrusion of basic and intermediate magmas into a high-grade metamorphic zone was coupled with D_2 transpressional deformation. Intrusions were accommodated into areas of high strain. A consequence of intrusion into a hot crustal domain is the strong interaction and hybridization of the magmas. A characteristic feature of the intrusive suite, which has calc-alkaline affinities, is a marked peraluminous composition for intermediate silica values, at which calc-alkaline rocks are normally metaluminous, denoting the effects of local assimilation of country metasedimentary rocks. By contrast, the Roses granodiorite, which is located far from the anatectic domains, retains unmodified calc-alkaline features. Local interactions between intrusive mafic magmas and migmatites are also responsible for the high CaO content of some leucosomes. In spite of these local interactions, mafic and intermediate rocks show geochemical features of arc magmatism (e.g. depletions in Nb and Ta). Migmatites and leucosomes are almost identical indicating the absence of fractionation of incompatible elements during anatexis, a common phenomenon in crustal migmatites that has been related to melting in disequilibrium and control of accessory minerals (e.g. apatite and zircon) leading to null mineral/melt partitioning (Bea, 1996; García-Arias, Corretgé & Castro, 2012). Leucogranites show depletion in incompatible elements (mostly in REEs, Y and Zr) with respect to migmatites and leucosomes, which is compatible with garnet retention as a peritectic restitic mineral in the solid residue left after partial melting of metasediments.

In summary, there are three relevant penecontemporaneous processes whose age can be estimated with geochronological data from this study: (i) intrusion of calc-alkaline magmas, (ii) D_2 deformation, since the analysed magmatic rocks are syntectonic with the D_2 tectonic event, and (iii) migmatization, because there is evidence that partial melting of high-grade schists was induced by the intrusion of quartz diorites and granitoids.

5.a. Timing of magmatism, deformation and migmatization in the Cap de Creus massif

The reported U–Pb zircon data yield igneous crystallization ages of 298.8 ± 3.8 Ma (Late Carboniferous – Early Permian) for the quartz diorite from the Tudela (north Cap de Creus) migmatitic complex and 290.8 ± 2.9 Ma (Early Permian) for the Roses granodiorite (Fig. 9). Crystallization ages of calc-alkaline magmatic rocks from the Cap de Creus are thus estimated to between *c*. 299 Ma and *c*. 291 Ma (Late Carboniferous – Early Permian). This is within the wider range of ages obtained for the calc-alkaline volcanic and plutonic rocks from the Central–Eastern Pyrenees (U–Pb zircon ages of *c*. 304–283 Ma; Pereira *et al.* 2014). When comparing the estimated ages from this study with the ages calculated for the neighbouring Sant Llorenç – La Jonquera pluton, it appears that they are in accordance with an age obtained for a syn-D_2 granodiorite (U–Pb age of *c*. 295 Ma; O. Maurel, unpub. Ph.D. thesis, Univ. Montpellier II, 2003), but differ significantly from the older ages obtained by Aguilar *et al.* (2013) for the equally syn-D_2 tonalites and gabbro-diorites (U–Pb ages of *c*. 314–311 Ma and 312–307 Ma, respectively). The Cap de Creus quartz diorite and granodiorite are also younger than the granodiorite-tonalites from Quérigut (U–Pb zircon age of 307 ± 2 Ma; Roberts *et al.* 2000). On the other hand, they appear to be slightly older than the Permian gabbroids and granitoids of the Montnegre massif, Catalan Coastal Ranges (^{40}Ar–^{39}Ar ages in the range of *c*. 291–285 Ma; Solé *et al.* 2002).

The obtained ages from this study are too young in regards to the published age estimates for the Variscan orogeny in the Pyrenean segment, which, according to Laumonier, Marignac & Kister (2010), extended from Namurian to Stephanian times (*c*. 325–300 Ma). Based on this scheme, the undeformed or almost undeformed granitoids from the Western Pyrenees and from the Catalan Coastal Ranges are actually consistent with a post-Variscan, Permian age. On the contrary, the syntectonic character of the Cap de Creus magmatic rocks (they are all syn- to late-D_2 and pre-D_3) is in apparent contradiction to these Permian ages. For the tectonomagmatic evolution of this part of the Variscan belt this poses a seeming problem, as the Cap de Creus has become a type locality in the context of progressive Variscan D_2–D_3 transpression (Druguet, 2001; Carreras *et al.* 2004). In view of the geochronological data of this study it can be inferred that the Variscan orogeny in the Eastern Pyrenean segment extended into the Lower Permian, and that by those times D_2 and D_3 ductile deformations did localize in this relatively more internal domain of the NE Iberian segment of the belt.

https://doi.org/10.1017/S0016756814000041 Published online by Cambridge University Press

In regard to the age of migmatization and thus development of the Cap de Creus migmatitic complexes, this could not be established by means of zircon geochronology. Metamorphic overgrowths dated in composite zircons from a migmatite and a leucosome only give Precambrian ages (this study). We also noted the presence of a very thin overgrowth, probably related to migmatization, but it has not been possible to date with SHRIMP. Migmatites and leucosomes are almost identical in terms of trace elements, reporting the absence of fractionation of incompatible elements during anatexis. This is compatible with a fast extraction of melts that prevent chemical re-equilibration, as it has been demonstrated by melting experiments (García-Arias, Corretgé & Castro, 2012). Quick melt segregation also likely impeded the formation of new zircon crystals. All analysed zircons from these migmatites are inherited from the metasedimentary protolith (Fig. 10). However, on the basis of field relationships indicative of a synchronism between intrusion of quartz diorites and granitoids, and partial melting of the enclosing schists, the age of migmatization can be very close to the age of emplacement and crystallization of the quartz diorite magmas at about 299 Ma (Fig. 9).

The zircons from the migmatite and the leucosome are characterized by: (i) a wide range of grain size, (ii) variable internal growth structures, (iii) distinct Th and U compositions, and (iv) scattered distributions of U–Pb ages. These features indicate that these zircons are detrital grains that have accumulated in a sedimentary protolith from one or more sources. The relative probability diagram with the inherited zircons analysed in this study (including three analyses from the Roses granodiorite) shows two main age clusters at *c*. 730–542 Ma and *c*. 2.9–2.2 Ga (Fig. 10). A range of inherited ages between 600 and 2740 Ma has also been obtained from migmatites from the nearby Roc de Frausa massif (Aguilar *et al.* 2013). A comparable distribution of detrital zircon ages was obtained for an Ediacaran metatuff from the southern Cap de Creus (Castiñeiras *et al.* 2008). The number of inherited age data (this study) is not enough to make great considerations on the provenance of detrital zircons, but may indicate some important crustal growth processes in North Gondwana which were already recognized in Ediacaran strata of Iberia (Schäfer *et al.* 1993; Fernández-Suárez, Gutiérrez-Alonso & Jeffries, 2002; Linnemann *et al*. 2008; Pereira *et al*. 2008, 2012*a,b*; Talavera *et al*. 2012; Fernández-Suárez *et al.* 2013). Concerning the recent compilation by Drost *et al.* (2011) of potential sources of North Gondwana that provided detritus to the peri-Gondwanan Ediacaran basins, the Cryogenian–Ediacaran detrital zircons found in the Cap de Creus strata probably indicate provenance from the active margin of North Gondwana with voluminous magmatic arcs. These Ediacaran basins would be located near the West African Craton, receiving detritus from inland regions of North Gondwana, such as the Arabian–Nubian shield and the Saharan Metacraton crossed by the Transgondwanan Supermountain and related superfan systems (Squire *et al*. 2006). Despite the limited number of data, it is appropriate to highlight the significant percentage of Palaeoproterozoic ages in the range *c*. 2.5–2.2 Ga (Rhyacian–Siderian), a fact that has so far been little explored for palaeogeographic reconstructions.

5.b. On the D_2 transpression and associated magmatism

The D_2 transpressional deformation in the Cap de Creus region was highly heterogeneously distributed, with preferred localization of high-strain zones inside the high-grade metamorphic areas (Druguet, 2001). The field and geochronological data presented in this work highlight the association between the D_2 structural evolution and the emplacement of mantle-derived calc-alkaline magmas in the more deformed areas, where high-grade metamorphism and anatectic processes were focused. A qualitative transpression model is proposed here to give an explanation to the most relevant features of the Cap de Creus region (Fig. 11). The studied region can be considered as being located at the southern boundary of a regional-scale transpressional shear zone, characterized by prominent deformation gradients and predominant N- and NE-dipping structures. The kinematics of such a shear zone entails a component of sub-vertical extrusion with associated shortening normal to the strike of the shear zone boundaries. Accordingly, previous sub-horizontal geological surfaces (e.g. metamorphic isograds) are uplifted inside the shear zone, with concomitant telescoping of metamorphic zones. This model can account for the rather sudden increase in the metamorphic degree from SSW to NNE, i.e. towards the interior of the shear zone, where high-grade metamorphic rocks became tectonically exhumed. Finally, the tectonic activity of the transpressional shear zone was accompanied by ascent of mantle-derived magmas, which exploited the pressure gradients reached inside the zone and the channels provided by minor structures. This also attests to the deep-seated nature of the regional structure, where the thermal effects of the intrusion of calc-alkaline magmas contributed to the uplifting and telescoping of metamorphic isograds (Fig. 11). Some minor magma batches (such as the Rodes and Roses stocks) could have ascended near the boundary of the regional-scale transpressional shear zone, reaching low-grade country rocks.

5.c. Setting of the geodynamic evolution of the basement segment of the Eastern Pyrenees

The essentially calc-alkaline compositions of the dated rocks suggest the implication of a mantle–crust mixed source with different degrees of additional crustal contamination for the parental magmas, a feature that is classically associated with continental arc magmatism. This can be linked to a recently published model by Pereira *et al.* (2014). According to these authors,

https://doi.org/10.1017/S0016756814000041 Published online by Cambridge University Press

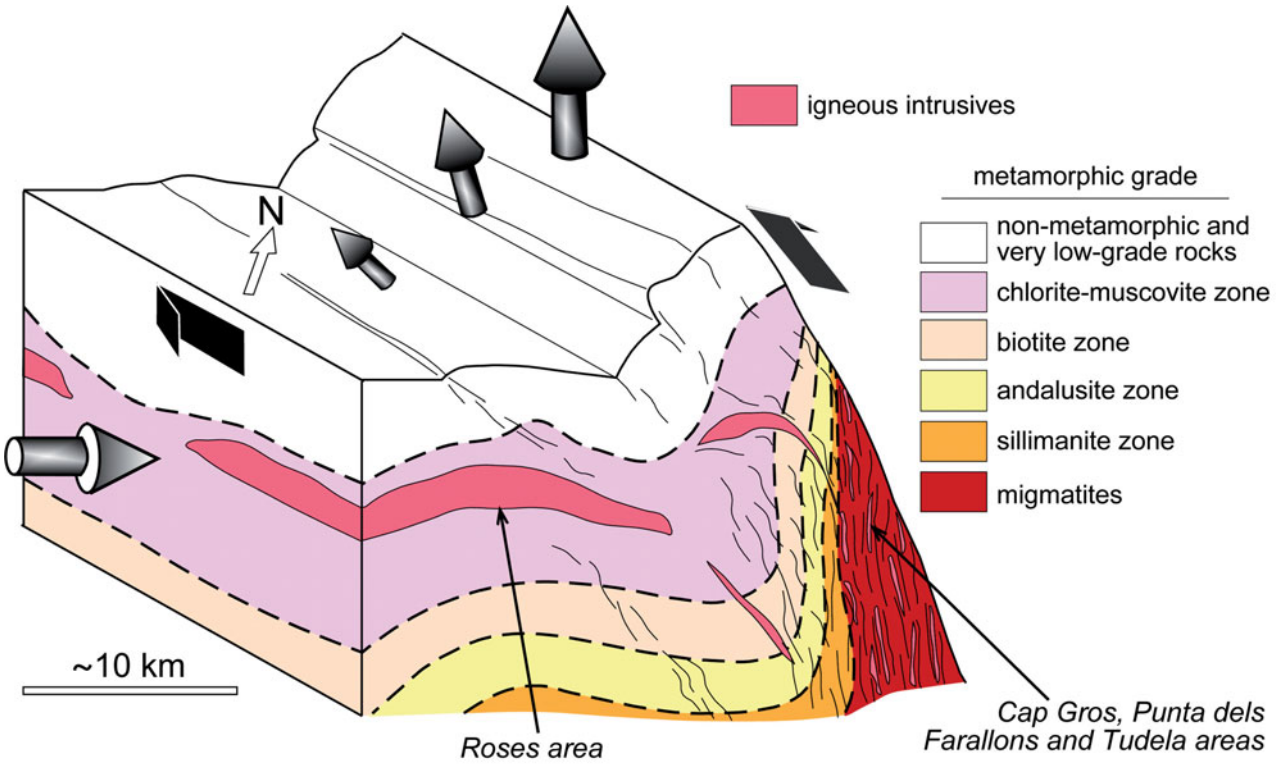

Figure 11. (Colour online) Schematic block-diagram (not to scale) proposed to qualitatively explain the transpressive nature of the D_2 phase in the Cap de Creus region, based on models in Druguet (2001) and Carreras & Druguet (2013). The D_2 deformation structures (illustrated with thin, curved lines) are more penetrative with depth. The kinematic pattern includes dextral strike-slip and reverse dip-slip simple-shear components (flat, black arrows), as well as shortening normal to the strike of the regional-scale shear zone and associated sub-vertical extrusion (cylindrical-conical arrows). Telescoping of metamorphic isograds inside the regional-scale shear zone is due to both the shortening-extrusion component, and the intrusion of calc-alkaline mantle-derived magmas. See main text for explanation.

volcanism and plutonism in the Variscan segment of the Pyrenees would be the result of arc magmatism caused by the northwestward subduction of the Palaeotethyan oceanic lithosphere below the margins of Pangaea during *c*. 304–283 Ma (see a reconstruction of the Variscan belt at *c*. 300 Ma in fig. 9 of Pereira *et al.* 2014). In a wider context, during Late Carboniferous time, the western zones of the Variscan belt were subjected to the Laurussia–Gondwana collision, whereas subduction of the Palaeotethyan ocean prevailed during and after Late Carboniferous – Early Permian times (Eo-Cimmerian cycle) along the eastern domains (Stampfli, vonRaumer, & Borel, 2002; Stampfli *et al.* 2013).

Stampfli, vonRaumer, & Borel, (2002) stated that 'the paleo-Tethys is more or less completely ignored by those who follow the classic Hercynian ideas', a fact that particularly applies to many works published on the Hercynides of Iberia. This way, prior to the work by Pereira *et al.* (2014), there are few exceptions where a Late Carboniferous – Early Permian subduction model is envisaged or discussed for the NE of Iberia. This hypothesis was already postulated by Enrique (1990) for the calc-alkaline magmas of the Catalan Coastal Ranges, interpreted by this author as generated in a convergent plate margin above the subducted oceanic lithosphere as in the case of volcanic arc magmas; and it was briefly hinted by Roberts *et al.* (2000) for the Pyrenean plutons.

An attempt can be made to correlate the tectonomagmatic evolution of Cap de Creus and the Eastern Pyrenees in the context of the Palaeotethyan subduction model so that, in these domains characterized by intense D_2–D_3 deformation, subduction-related magmatism would be coupled to localization of transpressional deformation. Oblique convergence along a subduction zone can be accommodated by transpression (McCaffrey, 1992). The active transpressional plate boundary of New Zealand (Furlong & Kamp, 2009) and the West Karamay Unit in Central Asia (Choulet *et al*. 2012) are clear examples of this link between subduction and transpressive zones. Transpression in the Eastern Pyrenean domain could also be in turn related to the formation of the late Variscan Iberian oroclines west and southwest of the study area (Gutiérrez-Alonso *et al.* 2011; Martínez Catalán, 2011).

In the Eastern Pyrenees, there is no evidence for crustal-scale extension in Late Carboniferous – Early Permian time, but localization of a syn-subduction deformation zone, which corresponds to a compression-dominated transpression (D_2) to strike-slip-dominated transpression (D_3), keeping a NNW–SSE crustal shortening direction. The Late Carboniferous – Early Permian grabens in the Central–Eastern Pyrenees could

https://doi.org/10.1017/S0016756814000041 Published online by Cambridge University Press

correspond to pull-apart structures associated with major strike-slip faults, which may be the surface equivalents of the ductile shear zones developed in the Variscan basement (Speksnijder, 1985).

6. Conclusions

Only two main ages have resulted from the present U–Pb zircon geochronological study from Cap de Creus, a small but key area to understanding the tectonothermal evolution of the basement of NE Iberia. Late Carboniferous – Early Permian (*c*. 299–291 Ma) crystallization ages have been estimated for calc-alkaline magmatic rocks. A quartz diorite from the north Cap de Creus Tudela migmatitic complex yielded an age of 298.8 ± 3.8 Ma and the Roses granodiorite 290.8 ± 2.9 Ma. Although all analysed zircons from the migmatites are inherited from the metasedimentary protolith, straightforward structural evidence allows us to postulate that migmatization and D_2 NNW–SSE transpressional deformation occurred within the same time span. Thus, magmatism in the Eastern Pyrenean segment was coeval with intense transpressional deformation, which may be considered late Variscan, Hercynian or early Cimmerian.

Most granitoids in NE Iberia are within a similar age interval, with those from the Catalan Coastal Ranges and Western Pyrenees looking post-tectonic because they are almost undeformed/unaffected by the pervasive D_2 transpression/D_3 late shearing that localized along the more internal Eastern Pyrenean domain.

A more systematic programme of dating would permit better constraint of the Cap de Creus tectonomagmatic processes, and this would include the dating of the latest intrusive rocks, i.e. the late-D_2 pegmatite dyke swarm, and the latest deformation structures attributed to the Variscan cycle, i.e. the D_3 shear zones.

Acknowledgements. Support for this work was provided by the Spanish MEC-MICINN, projects CGL2010-21751 and CGL2010-22022, by the Portuguese FCT, projects PTDC/CTE-GIX/110426/2009 and PTDC/GEO-GEO/2446/2012-FCOMP-01-0124-FEDER-029192), and by UNESCO-IUGS, project IGCP 597. We thank G. Ian Alsop and José R. Martínez Catalán for providing helpful comments on the manuscript.

References

Ábalos, B., Carreras, J., Druguet, E., Escuder Viruete, J., Gómez Pugnaire, M. T., Lorenzo Álvarez, S., Quesada, C., Rodríguez Fernández, R. & Gil-Ibarguchi, J. I. 2002. Variscan and pre-Variscan tectonics. In *The Geology of Spain* (eds W. Gibbons & M. T. Moreno), pp. 155–83. London: Geological Society of London.

Aguilar, C., Liesa, M., Castiñeiras, P. & Navidad, M. 2013. Late Variscan metamorphic and magmatic evolution in the eastern Pyrenees revealed by U–Pb age zircon dating. *Journal of the Geological Society, London*, published online 12 December 2013. doi: 10.1144/jgs2012-086.

Alfonso, P., Melgarejo, J. C., Yusta, I. & Velasco, F. 2003. Geochemistry of feldspars and muscovite in granitic pegmatite from the Cap de Creus field, Catalonia, Spain. *The Canadian Mineralogist* **41**, 103–16.

Autran, A., Fonteilles, M. & Guitard, G. 1970. Relations entre les intrusions de granitoides, l'anatexie, et le métamorphisme régional considerées principalment du point de vue de l'eau: cas de la Chaine hercynienne des Pyrénées Orientales. *Bulletin de la Société Géologique de France* **7**, 673–731.

Bea, F. 1996. Residence of REE, Y, Th and U in granites and crustal protoliths; implications for the chemistry of crustal melts. *Journal of Petrology* **37**, 521–52.

Carreras, J. 2001. Zooming on Northern Cap de Creus shear zones. *Journal of Structural Geology* **23**, 1457–86.

Carreras, J. & Capellà, I. 1994. Tectonic levels in the Palaeozoic basement of the Pyrenees: a review and a new interpretation. *Journal of Structural Geology* **16**, 1509–24.

Carreras, J. & Druguet, E. 2013. *Illustrated Field Guide to the Geology of Cap de Creus*. Servei de Publicacions de la Universitat Autònoma de Barcelona, 123 pp.

Carreras, J., Druguet, E., Griera, A. & Soldevila, J. 2004. Strain and deformation history in a syntectonic pluton. The case of the Roses granodiorite (Cap de Creus, Eastern Pyrenees). In *Flow Processes in Faults and Shear Zones* (eds G. I. Alsop, R. E. Holdsworth, K. J. W. McCaffrey & W. Hand), pp. 307–19. Geological Society of London, Special Publication no. 224.

Carreras, J. & Losantos, M. 1982. Geological setting of the Roses granodiorite (E-Pyrenees,Spain). *Acta geológica Hispánica* **17**(4), 219–25.

Castiñeiras, P., Navidad, M., Liesa, M., Carreras, J. & Casas, J. M. 2008. U–Pb zircon ages (SHRIMP) for Cadomian and Early Ordovician magmatism in the Eastern Pyrenees: new insights into the pre-Variscan evolution of the northern Gondwana margin. *Tectonophysics* **461**, 228–39.

Choulet, F., Faure, M., Cluzel, D., Chen, Y., Lin, W. & Wang, B. 2012. From oblique accretion to transpression in the evolution of the Altaid collage: new insights from West Junggar, northwestern China. *Gondwana Research* **21**, 530–47.

Cumming, G. L. & Richards, J. R. 1975. Ore lead isotope ratios in a continuously changing earth. *Earth and Planetary Science Letters* **28**, 155–71.

Damm, K., Harmon, R. S., Heppner, P. M. & Dornseipen, U. 1992. Stable isotope constraints of the Cabo de Creus garnet ± tourmaline pegmatites, massif des Alberes, Eastern Pyrenees, Spain. *Geological Journal* **27**, 76–86.

Debon, F., Enrique, P. & Autran, A. 1995. Magmatisme hercynien. In *Synthèse Géologique et Géophysique des Pyrénées. T.1: Cycle Hercynien* (eds A. Barnolas & J. C. Chiron), pp. 361–499. Orléans & Madrid: BRGM.

Debon, F. & Le Fort, P. 1983. A chemical-mineralogical classification of common plutonic rocks and associations. *Transactions of the Royal Society of Edinburgh: Earth Sciences* **73**, 135–49.

De la Roche, H. 1978. La chimie des roches présentée et interpretée d'aprés la structure de leur facies minéral dans l'espace des variables chimiques: fonctions spécifiques et diagrammes qui s'en déduisent – application aux roches ignées. *Chemical Geology* **21**, 63–87.

Denèle, Y., Olivier, P., Gleizes, G. & Barbey, P. 2009. Decoupling between the middle and upper crust during

transpression-related lateral flow: Variscan evolution of the Aston gneiss dome (Pyrenees, France). *Tectonophysics* **477**, 244–61.

DROST, K., GERDES, A., JEFFRIES, T., LINNEMANN, U. & STOREY, C. 2011. Provenance of Neoproterozoic and early Paleozoic siliciclastic rocks of the Teplá-Barrandian unit (Bohemian Massif): evidence from U–Pb detrital zircon ages. *Gondwana Research* **19**, 213–31.

DRUGUET, E. 2001. Development of high thermal gradients by coeval transpression and magmatism during the Variscan orogeny: insights from the Cap de Creus (Eastern Pyrenees). *Tectonophysics* **332**, 275–93.

DRUGUET, E., ALSOP, I. G. & CARRERAS, J. 2009. Coeval brittle and ductile structures associated with extreme deformation partitioning in a multilayer sequence. *Journal of Structural Geology* **31**, 498–511.

DRUGUET, E. & CARRERAS, J. 2006. Analogue modelling of syntectonic leucosomes in migmatitic schists. *Journal of Structural Geology* **28**, 1734–47.

DRUGUET, E., ENRIQUE, P. & GALÁN, G. 1995. Tipología de los granitoides y las rocas asociadas del complejo migmatítico de la Punta dels Farallons (Cap de Creus, Pirineo Oriental). *Geogaceta* **18**, 199–202.

DRUGUET, E. & HUTTON, D. H. W. 1998. Syntectonic anatexis and magmatism in a mid-crustal transpression shear zone: an example from the Hercynian rocks of the eastern Pyrenees. *Journal of Structural Geology* **20**, 905–16.

ENRIQUE, P. 1990. The Hercynian intrusive rocks of the Catalonian Coastal Ranges (NE Spain). *Acta Geológica Hispánica* **25**, 39–64.

ENRIQUE, P. 2002. Intrusive rocks of the Pyrenees and Catalonian Coastal Ranges. In *The Geology of Spain* (eds W. Gibbons & M. T. Moreno), pp. 141–7. London: Geological Society of London.

FERNÁNDEZ, C., BECCHIO, R., CASTRO, A., VIRAMONTE, J. M., MORENO-VENTAS, I. & CORRETGE, L. G. 2008. Massive generation of atypical ferrosilicic magmas along the Gondwana active margin: implications for cold plumes and back-arc magma generation. *Gondwana Research* **14**, 451–73.

FERNÁNDEZ-SUÁREZ, J., GUTIÉRREZ-ALONSO, G. & JEFFRIES, T. E. 2002. The importance of along-margin terrane transport in northern Gondwana: insights from detrital zircon parentage in Neoproterozoic rocks from Iberia and Brittany. *Earth and Planetary Science Letters* **204**, 75–88.

FERNÁNDEZ-SUÁREZ, J., GUTIÉRREZ-ALONSO, G., PASTOR-GALÁN, D., HOFMANN, M., MURPHY, J. B. & LINNEMANN, U. 2013. The Ediacaran-Early Cambrian detrital zircon record of NW Iberia: possible sources and paleogeographic constraints. *International Journal of Earth Sciences*, published online 16 June 2013. doi: 10.1007/s00531-013-0923-3.

FURLONG, K. P. & KAMP, P. J. J. 2009. The lithospheric geodynamics of plate boundary transpression in New Zealand: Initiating and emplacing subduction along the Hikurangi margin of New Zealand, and the Tectonic evolution of the Alpine Fault system. *Tectonophysics* **474**, 449–62.

GARCÍA-ARIAS, M., CORRETGÉ, L. G. & CASTRO, A. 2012. Trace element behaviour during partial melting of Iberian orthogneisses: an experimental study. *Chemical Geology* **292–293**, 1–17.

GLEIZES, G., LEBLANC, D. & BOUCHEZ, J. L. 1997. Variscan granites of the Pyrenees revisited: their role as syntectonic markers of the orogen. *Terra Nova* **9**, 38–41.

GLEIZES, G., LEBLANC, D. & BOUCHEZ, J. L. 1998. The main phase of the Hercynian orogeny of the Pyrenees is a dextral transpression. In *Continental Transpressional and Transtensional Tectonics* (eds R. E. Holdsworth, R. A. Strachan & J. F. Dewey), pp. 267–73. Geological Society of London, Special Publication no. 135.

GUTIÉRREZ-ALONSO, G., MURPHY, B., FERNÁNDEZ-SUÁREZ, J., WEIL, A. B., FRANCO, M. P. & GONZALO, J. C. 2011. Lithospheric delamination in the core of Pangea: Sm–Nd insights from the Iberian mantle. *Geology* **39**, 155–8.

HEAMAN, L. M., BOWINS, R. & CROCKET, J. 1990. The chemical composition of igneous zircon studies: implications for geochemical tracer studies. *Geochimica et Cosmochimica Acta* **64**, 1905–23.

KELEMEN, P. B., HANGHØJ, K. & GREENE, A. 2003. One view of the geochemistry of subduction-related magmatic arcs, with an emphasis on primitive andesite and lower crust. In *The Crust* (eds H. D. Holland, K. K. Turekian & R. L. Rudnick), pp. 593–659. Treatise on Geochemistry, Vol. 3. Oxford: Elsevier–Pergamon.

LAUMONIER, B., MARIGNAC, C. & KISTER, P. 2010. Polymetamorphism and crustal evolution of the eastern Pyrenees during the Late Carboniferous Variscan orogenesis. *Bulletin de la Société Géologique de France* **181**, 411–28.

LEBLANC, D., GLEIZES, G., ROUX, L. & BOUCHEZ, J. L. 1996. Variscan dextral transpression in the French Pyrenees: new data from the Pic des Trois-Seigneurs granodiorite and its country rocks. *Tectonophysics* **261**, 331–45.

LINNEMANN, U., PEREIRA, M. F., JEFFRIES, T., DROST, K. & GERDES, A. 2008. Cadomian Orogeny and the opening of the Rheic Ocean: New insights in the diacrony of geotectonic processes constrained by LA-ICP-MS U–Pb zircon dating (Ossa-Morena and Saxo-Thuringian Zones, Iberian and Bohemian Massifs). *Tectonophysics* **461**, 21–43.

MARTÍNEZ, F. J., RECHE, J. & IRIONDO, A. 2008. U–Pb Shrimp-RG zircon ages of Variscan igneous rocks from the Guilleries massif (NE Iberia pre-Mesozoic basement). Geological implications. *Comptes Rendus Geoscience* **340**, 223–32.

MARTÍNEZ CATALÁN, J. *R.* 2011. Are the oroclines of the Variscan belt related to late Variscan strike-slip tectonics? *Terra Nova* **23**, 241–7.

MCCAFFREY, R. 1992. Oblique plate convergence, slip vectors, and forearc deformation. *Journal of Geophysical Research* **97**, 8905–15.

NAKAMURA, N. 1974. Determination of REE, Ba, Fe, Mg, Na and K in carbonaceous and ordinary chondrites. *Geochimica et Cosmochimica Acta* **38**, 757–75.

OLIVIER, PH., GLEIZES, G. & PAQUETTE, J. L. 2004. Gneiss domes and granite emplacement in an obliquely convergent regime: new interpretation of the Variscan Agly Massif (Eastern Pyrenees, France). In *Gneiss Domes in Orogeny* (eds D. L. Whitney, C. Teyssier & C. S. Siddoway), pp. 229–242. Geological Society of America, Special Paper no. 380.

OLIVIER, PH., GLEIZES, G., PAQUETTE, J. L. & MUÑOZ SÁEZ, C. 2008. Structure and U-Pb dating of the Saint-Arnac pluton and the Ansignan charnockite (Agly massif): a cross section from the upper to the middle crust of the Variscan Eastern Pyrenees. *Journal of the Geological Society* **165**, 141–52.

PEREIRA, M. F., CASTRO, A., CHICHORRO, M., FERNÁNDEZ, C., DÍAZ-ALVARADO, J., MARTÍ, M. & RODRÍGUEZ, C. 2014. Chronological link between deep-seated processes in magma chambers and eruptions: Permo-Carboniferous magmatism in the core of Pangaea (Southern Pyrenees). *Gondwana Research* **25**, 290–308.

PEREIRA, M. F., CHICHORRO, M., WILLIAMS, I. S. & SILVA, J. B. 2008. Zircon U-Pb geochronology of paragneisses and biotite granites from the SW Iberian Massif (Portugal): evidence for a paleogeographic link between the Ossa-Morena Ediacaran basins and the West African craton, In *The Boundaries of the West African Craton* (eds J. P. Liégeois & E. Nasser), pp. 385–408. Geological Society of London, Special Publication no. 297.

PEREIRA, M. F., LINNEMANN, U., HOFMANN, M., CHICHORRO, M., SOLA, A. R., MEDINA, J. & SILVA, J. B. 2012*a*. The provenance of Late Ediacaran and Early Ordovician siliciclastic rocks in the Southwest Central Iberian Zone: constraints from detrital zircon data on northern Gondwana margin evolution during the late Neoproterozoic. *Precambrian Research* **192–195**, 166–89.

PEREIRA, M. F., SOLA, A. R., CHICHORRO, M., LOPES, L., GERDES, A. & SILVA, J. B. 2012 *b*. North-Gondwana assembly, break-up and paleogeography: U–Pb isotope evidence from detrital and igneous zircons of Ediacaran and Cambrian rocks of SW Iberia. *Gondwana Research* **22**, 866–81.

ROBERTS, M. P., PIN, C., CLEMENS, J. D. & PAQUETTE, J. L. 2000. Petrogenesis of mafic to felsic plutonic rock associations: the calc-alkaline Quérigut complex, French Pyrenees. *Journal of Petrology* **41**, 809–44.

SCHÄFFER, H. J., GEBAUER, D., NÄGLER, T. F. & EGUILUZ, L. 1993. Conventional and ion-microprobe U-Pb dating of detrital zircons of the Tentudia Group (Serie Negra SW Spain): implications for zircon systematics, stratigraphy, tectonics and the Precambrian/Cambrian boundary. *Contributions to Mineralogy and Petrology* **113**, 289–99.

SOLÉ, J., COSCA, M., SHARP, Z. & ENRIQUE, P. 2002. 40Ar/39Ar geochronology and stable isotope geochemistry of late-Hercynian intrusions from north-eastern Iberia with implications for argon loss in K-feldspar. *International Journal of Earth Sciences* **91**, 865–81.

SPEKSNIJDER, A. 1985. Anatomy of a strike-slip fault controlled sedimentary basin, Permian of the Southern Pyrenees, Spain. *Sedimentary Geology* **44**, 179–223.

SQUIRE, R. J., CAMPBELL, I. H., ALLEN, C. M. & WILSON, C. J. L. 2006. Did the Transgondwanan Supermountain trigger the explosive radiation of animals on Earth? *Earth and Planetary Science Letters* **250**, 116–33.

STAMPFLI, G. M., HOCHARD, C., VÉRARD, C., WILHEM, C. & VONRAUMER, J. 2013. The formation of Pangea. *Tectonophysics* **593**, 1–19.

STAMPFLI, G. M., VONRAUMER, J. F. & BOREL, G. D. 2002. Paleozoic evolution of pre-Variscan terranes: from Gondwana to the Variscan collision. In *Variscan-Appalachian Dynamics: The Building of the Late Paleozoic Basement* (eds J. R. Martínez Catalán, R. D. Hatcher, Jr., R. Arenas & F. Díaz García), pp. 263–80. Geological Society of America, Special Paper no. 364.

STEIGER, R. H. & JÄGER, E. 1977. Subcommission on geochronology: convention on the use of decay constants in geo- and cosmochronology. *Earth and Planetary Science Letters* **36**, 359–62.

TALAVERA, C., MONTERO, P., MARTÍNEZ POYATOS, D. & WILLIAMS, I. S. 2012. Ediacaran to Lower Ordovician age for rocks ascribed to the Schist–Graywacke Complex (Iberian Massif, Spain): Evidence from detrital zircon SHRIMP U–Pb geochronology. *Gondwana Research* **22**, 928–42.

VILÀ, M., PIN, C., ENRIQUE, P. & LIESA, M. 2005. Telescoping of three distinct magmatic suites in an orogenic setting: generation of Hercynian igneous rocks of the Albera Massif (Eastern Pyrenees). *Lithos* **83**, 97–127.

WILLIAMS, I. S. & CLAESSON, S. 1987. Isotopic evidence for the Precambrian provenance and Caledonian metamorphism of high grade paragneisses from the Seve Nappes, Scandinavian Caledonides. *Contributions to Mineralogy and Petrology* **97**, 205–17.

https://doi.org/10.1017/S0016756814000041 Published online by Cambridge University Press